Weak decay of hypernuclei

W. M. Alberico and G. Garbarino

Dipartimento di Fisica Teorica, Università di Torino and INFN, Sezione di Torino, I–10125 Torino, Italy

1. – Introduction

The focus of these lectures is on the weak decay modes of hypernuclei, with special attention to Λ–hypernuclei. The subject involves many fields of modern theoretical and experimental physics, from nuclear structure to the fundamental constituents of matter and their interactions. The peculiar behaviour of matter containing strange quarks has raised in recent years many interesting problems, one of which being the physics of hypernuclei.

Hypernuclear physics was born in 1952, when the first hypernucleus was observed through its decays [1]. Since then, it has been characterized by more and more new challenging questions and answers. The interest was further raised by the great advances made in the last 15–20 years. Moreover, the existence of hypernuclei gives a new dimension to the traditional world of nuclei (states with new symmetries, selection rules, etc). They represent the first kind of *flavoured nuclei*, in the direction of other exotic systems (charmed nuclei and so on).

Hyperons (Λ, Σ, Ξ, Ω) have lifetimes of the order of 10^{-10} sec (apart from the Σ^0, which decays into $\Lambda\gamma$). They decay weakly, with a mean free path $\lambda \approx c\tau = \mathcal{O}(10 \text{ cm})$. A hypernucleus is a bound system of neutrons, protons and one or more hyperons. We will denote with $^{A+1}_{Y}Z$ a hypernucleus with Z protons, $A-Z$ neutrons and a hyperon Y. In order to describe the structure of these *strange nuclei* it is crucial the knowledge of the elementary hyperon–nucleon (YN) and hyperon–hyperon (YY) interactions. Hyperon masses differ remarkably from the nucleonic mass, hence the flavour $SU(3)$ symmetry is broken. The amount of this breaking is a fundamental question in order to understand

the baryon–baryon interaction in the strange sector.

Nowadays, the knowledge of hypernuclear phenomena is rather good, but some open problems still remain. The study of this field may help in understanding some important questions, related to:

1. some aspects of the baryon–baryon weak interactions;

2. the YN and YY strong interactions in the $J^P = 1/2^+$ baryon octet;

3. the possible existence of di–baryon particles;

4. the renormalization of hyperon and meson properties in the nuclear medium;

5. the nuclear structure: for instance, the long standing question of the origin of the spin–orbit interaction and other aspects of the many–body nuclear dynamics;

6. the role played by quark degrees of freedom, flavour symmetry and chiral models in nuclear and hypernuclear phenomena.

Many of these aspects can be discussed and understood by investigating the hypernuclear weak decays. Important related arguments, which here will not be considered or only briefly mentioned, can be found in the lectures by A. Gal [2] and T. Nagae [3], while the experimental viewpoint on the same subject is presented by H. Outa [4].

In these lectures the various weak decay modes of Λ–hypernuclei are described: indeed in a nucleus the Λ can decay by emitting a nucleon and a pion (*mesonic mode*) as it happens in free space, but its (weak) interaction with the nucleons opens new channels, customarily indicated as *non–mesonic* decay modes. These are the dominant decay channels of medium–heavy nuclei, where, on the contrary, the mesonic decay is disfavoured by Pauli blocking effect on the outgoing nucleon. In particular, one can distinguish between one–body and two–body induced decays, according whether the hyperon interacts with a single nucleon or with a pair of correlated nucleons.

An interesting rule for the amount of isospin violation ($\Delta I = 1/2$) is strongly suggested by the mesonic decay of free Λ's, whose branching ratios are almost in the proportion 2 to 1, according whether a $\pi^- p$ or $\pi^0 n$ are emitted. This totally empirical rule has been generally adopted in most of the models proposed for the evaluation of the Λ–hypernuclei decay widths: some of the expected consequences, however, seem to require additional work and investigation. Indeed, the total non–mesonic ($\Gamma_{\rm NM} = \Gamma_n + \Gamma_p \, (+\Gamma_2)$) and mesonic ($\Gamma_{\rm M} = \Gamma_{\pi^0} + \Gamma_{\pi^-}$) decay rates are well explained by several calculations; however, for many years the main open problem in the decay of Λ–hypernuclei has been the discrepancy between theoretical and experimental values of the ratio Γ_n/Γ_p. This topic will be discussed at length here, together with the most recent indications toward a solution of the puzzle.

Another interesting and open question concerns the asymmetric non–mesonic decay of polarized hypernuclei: strong inconsistencies appear already among data. Also in this case, as for the Γ_n/Γ_p puzzle, one can expect important progress from the present

and future improved experiments, which will provide a guidance for a deeper theoretical understanding of hypernuclear dynamics and decay mechanisms.

For a comprehensive review on the subject of these lectures we refer the reader to Ref. [5] and references therein.

2. – Weak decay modes of Λ–hypernuclei

In the production of hypernuclei, the populated state may be highly excited, above one or more threshold energies for particle decays. These states are unstable with respect to the emission of the hyperon, of photons and nucleons. The spectroscopic studies of strong and electromagnetic de–excitations give information on the hypernuclear structure which are complementary to those we can extract from excitation functions and angular distributions studies. Once the hypernucleus is stable with respect to electromagnetic and strong processes, it is in the ground state, with the hyperon in the $1s$ level, and can only decay via a strangeness–changing weak interaction, through the disappearance of the hyperon.

2˙1. *Mesonic decay*. – The mesonic mode is the main decay channel of a Λ in free space:

$$\begin{aligned} \Lambda \quad &\rightarrow \quad \pi^- p \quad &(\text{B.R.} = 63.9 \times 10^{-2}) \\ & \quad \pi^0 n \quad &(\text{B.R.} = 35.8 \times 10^{-2}) \end{aligned}$$

with a lifetime $\tau_\Lambda^{\text{free}} \equiv \hbar/\Gamma_\Lambda^{\text{free}} = 2.632 \times 10^{-10}$ sec.

Semi–leptonic and weak radiative Λ decay modes have negligible branching ratios:

$$\begin{aligned} \Lambda \quad &\rightarrow \quad n\gamma \quad &(\text{B.R.} = 1.75 \times 10^{-3}) \\ & \quad p\pi^-\gamma \quad &(\text{B.R.} = 8.4 \times 10^{-4}) \\ & \quad pe^-\overline{\nu}_e \quad &(\text{B.R.} = 8.32 \times 10^{-4}) \\ & \quad p\mu^-\overline{\nu}_\mu \quad &(\text{B.R.} = 1.57 \times 10^{-4}) \end{aligned}$$

and will not be considered here.

The Λ hyperon is an isospin singlet ($I_\Lambda = 0$), while the πN system can be either in $I = 1/2$ or in $I = 3/2$ isospin states. The customary angular momentum coupling implies:

$$\begin{aligned} |\pi^- p\rangle &= \sqrt{\frac{1}{3}} \left| \frac{3}{2}, -\frac{1}{2} \right\rangle - \sqrt{\frac{2}{3}} \left| \frac{1}{2}, -\frac{1}{2} \right\rangle, \\ |\pi^0 n\rangle &= \sqrt{\frac{2}{3}} \left| \frac{3}{2}, -\frac{1}{2} \right\rangle + \sqrt{\frac{1}{3}} \left| \frac{1}{2}, -\frac{1}{2} \right\rangle. \end{aligned}$$

Hence the ratio of amplitudes for $\Delta I = 1/2$ transitions yields:

$$\frac{\Gamma_{\Lambda \to \pi^- p}^{\text{free}}}{\Gamma_{\Lambda \to \pi^0 n}^{\text{free}}} \simeq \frac{\left| \langle \pi^- p | T_{1/2,-1/2} | \Lambda \rangle \right|^2}{\left| \langle \pi^0 n | T_{1/2,-1/2} | \Lambda \rangle \right|^2} = \left| \frac{\sqrt{2/3}}{\sqrt{1/3}} \right|^2 = 2,$$

while a $\Delta I = 3/2$ process should give:

$$\frac{\Gamma^{\text{free}}_{\Lambda \to \pi^- p}}{\Gamma^{\text{free}}_{\Lambda \to \pi^0 n}} \simeq \frac{\left| \langle \pi^- p | T_{3/2,-1/2} | \Lambda \rangle \right|^2}{\left| \langle \pi^0 n | T_{3/2,-1/2} | \Lambda \rangle \right|^2} = \left| \frac{\sqrt{1/3}}{\sqrt{2/3}} \right|^2 = \frac{1}{2}.$$

Experimentally the above ratio turns out to be:

$$\left\{ \frac{\Gamma^{\text{free}}_{\Lambda \to \pi^- p}}{\Gamma^{\text{free}}_{\Lambda \to \pi^0 n}} \right\}^{\text{Exp}} \simeq 1.78,$$

which is very close to 2 and strongly suggests the $\Delta I = 1/2$ rule on the isospin change. From the above considerations and from analyses of the Λ polarization observables it follows that the measured ratio between $\Delta I = 1/2$ and $\Delta I = 3/2$ transition amplitudes is very large:

$$\left| \frac{A_{1/2}}{A_{3/2}} \right| \simeq 30.$$

The $\Delta I = 1/2$ rule is based on experimental observations but its dynamical origin is not yet understood on theoretical grounds. It is also valid for the decay of the Σ hyperon and for pionic kaon decays (namely in non–leptonic strangeness–changing processes). Actually, this rule is slightly violated in the Λ free decay, and it is not clear whether it is a universal characteristic of all non–leptonic processes with $\Delta S \neq 0$. The Λ free decay in the Standard Model can occur through both $\Delta I = 1/2$ and $\Delta I = 3/2$ transitions, with comparable strengths: an s quark converts into a u quark through the exchange of a W boson. Moreover, the effective 4–quark weak interaction derived from the Standard Model including perturbative QCD corrections gives too small $|A_{1/2}/A_{3/2}|$ ratios ($\simeq 3 \div 4$, as calculated at the hadronic scale of about 1 GeV by using renormalization group techniques [6]). Therefore, non–perturbative QCD effects at low energy (such as hadron structure and reaction mechanism), which are more difficult to handle, and/or final state interactions could be responsible for the enhancement of the $\Delta I = 1/2$ amplitude and/or the suppression of the $\Delta I = 3/2$ amplitude[1].

The Q–value for free–Λ mesonic decay at rest is $Q_\Lambda \simeq m_\Lambda - m_N - m_\pi \simeq 40$ MeV. Then, taking into account energy–momentum conservation, $m_\Lambda \simeq \sqrt{\vec{p}^2 + m_\pi^2} + \sqrt{\vec{p}^2 + m_N^2}$ in the center–of–mass system and the momentum of the final nucleon turns out to be $p \simeq 100$ MeV. Inside a hypernucleus, the binding energies of the recoil nucleon ($B_N \simeq -8$ MeV) and of the Λ ($B_\Lambda \geq -27$ MeV) tend to further decrease Q_Λ [$Q_{\Lambda,\text{bound}} = Q_\Lambda + B_\Lambda - B_N$] and hence p.

As a consequence, in nuclei the Λ mesonic decay is disfavoured by the Pauli principle, particularly in heavy systems. It is strictly forbidden in normal infinite nuclear matter

---

[1] See, for example, a recent work based on the Instanton Liquid Model [7]

(where the Fermi momentum is $k_F^0 \simeq 270$ MeV), while in finite nuclei it can occur because of three important effects:

1. In nuclei the hyperon has a momentum distribution (being confined in a limited spatial region) that allows larger momenta to be available to the final nucleon;

2. The final pion feels an attraction by the medium such that for fixed momentum $\vec{q}$ it has an energy smaller than the free one $[\omega(\vec{q}) < \sqrt{\vec{q}^2 + m_\pi^2}]$, and consequently, due to energy conservation, the final nucleon again has more chance to come out above the Fermi surface. Indeed it has been shown [8, 9] that the pion distortion increases the mesonic width by one or two orders of magnitude for very heavy hypernuclei ($A \simeq 200$) with respect to the value obtained without the medium distortion;

3. At the nuclear surface the local Fermi momentum is considerably smaller than k_F^0, and the Pauli blocking is less effective in forbidding the decay.

In any case the mesonic width rapidly decreases as the nuclear mass number A of the hypernucleus increases.

The mesonic channel also gives information on the pion–nucleus optical potential since $\Gamma_{\mathrm{M}} = \Gamma_{\pi^-} + \Gamma_{\pi^0}$ is very sensitive to the pion self–energy in the medium: the latter is enhanced by the attractive P–wave π–nucleus interaction and reduced by the repulsive S–wave one. Evidence for a central repulsion in the Λ–nucleus mean potential was obtained from the mesonic decays of s–shell hypernuclei [10, 11].

2$\cdot$2. *Non–mesonic decay.* – In hypernuclei the weak decay can occur through processes which involve a weak interaction of the Λ with one or more nucleons. Sticking to the weak hadronic vertex $\Lambda \to \pi N$, when the emitted pion is virtual, then it will be absorbed by the nuclear medium, resulting in a non–mesonic process of the following type:

$$\text{(1)} \qquad\qquad\qquad\qquad \Lambda n \to nn \quad (\Gamma_n),$$
$$\text{(2)} \qquad\qquad\qquad\qquad \Lambda p \to np \quad (\Gamma_p),$$
$$\text{(3)} \qquad\qquad\qquad\qquad \Lambda NN \to nNN \quad (\Gamma_2).$$

The total weak decay rate of a Λ–hypernucleus is then:

$$\Gamma_{\mathrm{T}} = \Gamma_{\mathrm{M}} + \Gamma_{\mathrm{NM}},$$

where:

$$\Gamma_{\mathrm{M}} = \Gamma_{\pi^-} + \Gamma_{\pi^0}, \quad \Gamma_{\mathrm{NM}} = \Gamma_1 + \Gamma_2, \quad \Gamma_1 = \Gamma_n + \Gamma_p,$$

and the lifetime is $\tau = \hbar/\Gamma_{\mathrm{T}}$. The channel (3) can be interpreted by assuming that the pion is absorbed by a pair of nucleons, correlated by the strong interaction. Obviously, the non–mesonic processes can also be mediated by the exchange of more massive mesons than the pion (see figure 1).
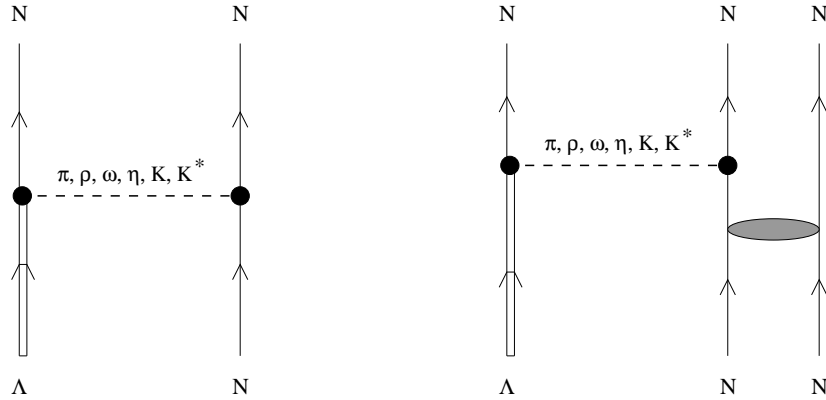
Fig. 1. – One–nucleon (a) and two–nucleon (b) induced Λ decay in nuclei.

The non–mesonic mode is *only possible in nuclei* and, nowadays, the systematic study of the hypernuclear decay is the only practical way to get information on the weak process $\Lambda N \to NN$ (which provides the first extension of the weak $\Delta S = 0\ NN \to NN$ interaction to strange baryons), especially on its parity–conserving part, which is masked by the strong interaction in the weak $NN \to NN$ reaction.

The final nucleons in the non–mesonic processes emerge with large momenta: disregarding the Λ and nucleon binding energies and assuming the available energy $Q = m_\Lambda - m_N \simeq 176$ MeV to be equally splitted among the final nucleons, it turns out that $p_N \simeq 420$ MeV for the one–nucleon induced channels [Eqs. (1), (2)] and $p_N \simeq 340$ MeV in the case of the two–nucleon induced mechanism [Eq. (3)]. Therefore, the non–mesonic decay mode is not forbidden by the Pauli principle: on the contrary, the final nucleons have great probability to escape from the nucleus. The non–mesonic mechanism dominates over the mesonic mode for all but the s–shell hypernuclei. Only for very light systems the two decay modes are competitive.

Since the non–mesonic channel is characterized by large momentum transfer, the details of the hypernuclear structure do not have a substantial influence (then providing useful information directly on the hadronic weak interaction). On the other hand, the NN and ΛN short range correlations turn out to be very important.

It is interesting to observe that there is an anticorrelation between mesonic and non–mesonic decay modes such that the experimental lifetime is quite stable from light to heavy hypernuclei [12, 13], apart from some fluctuation in light systems because of shell structure effects: $\tau_\Lambda = (0.5 \div 1)\,\tau_\Lambda^{\rm free}$. Since the mesonic width is less than 1% of the total width for $A > 100$, the above consideration implies that the non–mesonic rate is rather constant in the region of heavy hypernuclei.

This can be simply understood from the following consideration. If one naively assumes a zero range approximation for the non–mesonic weak interaction $\Lambda N \to nN$, then
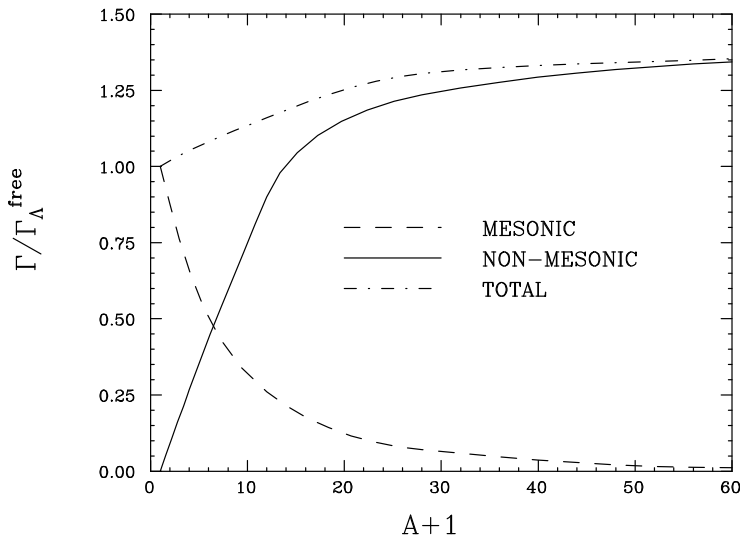
Fig. 2. – Qualitative behaviour of mesonic, non–mesonic and total decay widths as a function of the hypernuclear baryonic number $A + 1$.

Γ_1 is proportional to the overlap between the Λ wave function and the nuclear density:

$$\Gamma_1(A) \propto \int d\vec{r}\, |\psi_\Lambda(\vec{r})|^2 \rho_A(\vec{r}),$$

where the Λ wave function ψ_Λ (nuclear density ρ_A) is normalized to unity (to the nuclear mass number A). This overlap integral increases with the mass number and reaches a constant value: by using, e.g., Λ harmonic oscillator wave functions (with frequency ω adjusted to the experimental hyperon levels in hypernuclei) and Fermi distributions for the nuclear densities, we find $\Gamma_1(^{12}_\Lambda\mathrm{C})/\Gamma_1(^{208}_\Lambda\mathrm{Pb}) \simeq 0.56$, while Γ_1 is 90 % of the saturation value for $A \simeq 65$. In figure 2 the qualitative behaviour of mesonic, non–mesonic and total widths as a function of the nuclear mass number A is shown.

For $A \leq 11$ the experimental data are quite well fitted by $\Gamma_{\mathrm{NM}}/\Gamma_\Lambda^{\mathrm{free}} \simeq 0.1A$: Γ_1 is proportional to the number of ΛN pairs, A, as it is expected from the above simple description, where we neglect the contribution of Γ_2. However, Γ_1 saturates when the radius of the hypernucleus becomes sensitively larger than the range of the $\Lambda N \to nN$ interaction. For a more quantitative explanation it will be important to collect data with good precision. Yet, from the available data one can roughly say that the long distance component of the $\Lambda N \to nN$ transition has a range of about 1.5 fm and corresponds, as we expect, to the one–pion–exchange component of the interaction.

2˙3. *The Γ_n/Γ_p puzzle.* – Nowadays, an important question concerning the weak decay rates is the longstanding disagreement between theoretical estimates and experimental determinations of the ratio Γ_n/Γ_p between the neutron– and the proton–induced decay widths.

This problem will be extensively discussed in Section **5**. However, it is worth recalling here that, up to short time ago, all theoretical calculations appeared to strongly underestimate the available central data measured in several hypernuclei:

$$\left\{\frac{\Gamma_n}{\Gamma_p}\right\}^{\text{Th}} \ll \left\{\frac{\Gamma_n}{\Gamma_p}\right\}^{\text{Exp}}, \qquad 0.5 \lesssim \left\{\frac{\Gamma_n}{\Gamma_p}\right\}^{\text{Exp}} \lesssim 2.$$

Until recently the data were quite limited and not precise because of the difficulty in detecting the products of the non–mesonic decays, especially the neutrons. Moreover, the experimental energy resolution for the detection of the outgoing nucleons does not allow to identify the final state of the residual nuclei in the processes $^A_\Lambda Z \to {}^{A-2}Z + nn$ and $^A_\Lambda Z \to {}^{A-2}(Z-1) + np$. As a consequence, the measurements supply decay rates averaged over several nuclear final states.

In the one–pion–exchange (OPE) approximation, by assuming the $\Delta I = 1/2$ rule in the $\Lambda \to \pi^- p$ and $\Lambda \to \pi^0 n$ free couplings, the calculations (which will be reported later) give small ratios, in the range $0.05 \div 0.20$ for all the considered systems. However, as we shall see in Section **4**, the OPE model with $\Delta I = 1/2$ couplings has been able to reproduce the one–body stimulated non–mesonic rates $\Gamma_1 = \Gamma_n + \Gamma_p$ for light and medium hypernuclei. Hence, the problem seems to consist in overestimating the proton–induced and underestimating the neutron–induced transition rates.

In order to solve this puzzle (namely to explain both $\Gamma_n + \Gamma_p$ and Γ_n/Γ_p), many attempts have been made up to now, mainly without success. We recall the inclusion in the $\Lambda N \to nN$ transition potential of mesons heavier than the pion (also including the exchange of correlated or uncorrelated two–pions) [14–18], the inclusion of interaction terms that explicitly violate the $\Delta I = 1/2$ rule [19] and the description of the short range baryon–baryon interaction in terms of quark degrees of freedom [20, 21], which automatically introduces $\Delta I = 3/2$ contributions.

3. – Theoretical models for the decay rates

We illustrate here the theoretical approaches which have been utilized for the formal derivation of Λ decay rates in nuclei. We discuss first the general features of the approach used for direct finite nucleus calculations. It is usually called Wave Function Method (WFM), since it makes use of shell model nuclear and hypernuclear wave functions (both at hadronic and quark level) as well as pion wave functions generated by pion–nucleus optical potentials. Then we consider the Polarization Propagator Method (PPM), which relies on a many–body description of the hyperon self–energy in nuclear matter. The Local Density Approximation allows then one to implement the calculation in finite nuclei. Finally, a microscopic approach, based again on the PPM, is shortly sketched: in

this case the full Λ self–energy is evaluated on the basis of Feynman diagrams, which are derived, within a functional integral approach, in the framework of the so–called bosonic loop expansion.

$3^{.}1$. *Wave Function Method: mesonic width*. – The weak effective Hamiltonian for the $\Lambda \to \pi N$ decay can be parameterized in the form:

$$(4) \qquad \mathcal{H}^W_{\Lambda \pi N} = iGm^2_\pi \overline{\psi}_N (A + B\gamma_5) \vec{\tau} \cdot \vec{\phi}_\pi \psi_\Lambda,$$

where the values of the weak coupling constants $G = 2.211 \times 10^{-7}/m^2_\pi$, $A = 1.06$ and $B = -7.10$ are fixed on the free Λ decay. The constants A and B determine the strengths of the parity violating and parity conserving $\Lambda \to \pi N$ amplitudes, respectively. In order to enforce the $\Delta I = 1/2$ rule (which fixes $\Gamma^{\text{free}}_{\pi^-}/\Gamma^{\text{free}}_{\pi^0} = 2$), in Eq. (4) the hyperon is assumed to be an isospin spurion with $I = 1/2$, $I_z = -1/2$.

In the non–relativistic approximation, the free Λ decay width $\Gamma^{\text{free}}_\Lambda = \Gamma^{\text{free}}_{\pi^-} + \Gamma^{\text{free}}_{\pi^0}$ is given by:

$$\Gamma^{\text{free}}_\alpha = c_\alpha (Gm^2_\pi)^2 \int \frac{d\vec{q}}{(2\pi)^3 \, 2\omega(\vec{q})} \, 2\pi \, \delta[m_\Lambda - \omega(\vec{q}) - E_N] \left(S^2 + \frac{P^2}{m^2_\pi} \vec{q}^{\,2} \right),$$

where $c_\alpha = 1$ for Γ_{π^0} and $c_\alpha = 2$ for Γ_{π^-} (expressing the $\Delta I = 1/2$ rule), $S = A$, $P = m_\pi B/(2m_N)$, whereas E_N and $\omega(\vec{q})$ are the total energies of nucleon and pion, respectively. One finds the well known result:

$$\Gamma^{\text{free}}_\alpha = c_\alpha (Gm^2_\pi)^2 \frac{1}{2\pi} \frac{m_N q_{\text{c.m.}}}{m_\Lambda} \left(S^2 + \frac{P^2}{m^2_\pi} q^2_{\text{c.m.}} \right),$$

which reproduces the observed rates. In the previous equation, $q_{\text{c.m.}} \simeq 100$ MeV is the pion momentum in the center–of–mass frame.

In a finite nucleus approach, the *mesonic width* $\Gamma_{\text{M}} = \Gamma_{\pi^-} + \Gamma_{\pi^0}$ can be calculated by means of the following formula [8, 9]:

$$\Gamma_\alpha = c_\alpha (Gm^2_\pi)^2 \sum_{N \notin F} \int \frac{d\vec{q}}{(2\pi)^3 \, 2\omega(\vec{q})} \, 2\pi \, \delta[E_\Lambda - \omega(\vec{q}) - E_N]$$

$$\times \left\{ S^2 \left| \int d\vec{r}\phi_\Lambda(\vec{r})\phi_\pi(\vec{q},\vec{r})\phi^*_N(\vec{r}) \right|^2 + \frac{P^2}{m^2_\pi} \left| \int d\vec{r}\phi_\Lambda(\vec{r})\vec{\nabla}\phi_\pi(\vec{q},\vec{r})\phi^*_N(\vec{r}) \right|^2 \right\},$$

where the sum runs over non–occupied nucleonic states and E_Λ is the hyperon total energy. The Λ and nucleon wave functions ϕ_Λ and ϕ_N are obtainable within a shell model. The pion wave function ϕ_π corresponds to an outgoing wave, solution of the Klein–Gordon equation with the appropriate pion–nucleus optical potential V_{opt}:

$$\left\{ \vec{\nabla}^2 - m^2_\pi - 2\omega V_{\text{opt}}(\vec{r}) + [\omega - V_C(\vec{r})]^2 \right\} \phi_\pi(\vec{q},\vec{r}) = 0,$$

where $V_C(\vec{r})$ is the nuclear Coulomb potential and the energy eigenvalue ω depends on $\vec{q}$.

Different calculations [8, 9] have shown how strongly the mesonic decay is sensitive to the pion–nucleus optical potential, which can be parameterized in terms of the nuclear density, as discussed in Refs. [9], or evaluated microscopically, as in Ref. [8].

3'2. *Wave Function Method: non–mesonic width*. – Within the one–meson–exchange (OME) mechanism, the weak transition $\Lambda N \to nN$ is assumed to proceed via the mediation of virtual mesons of the pseudoscalar (π, η and K) and vector (ρ, ω and K^*) octets [14, 15] (see Fig 1).

The fundamental ingredients for the calculation of the $\Lambda N \to nN$ transition within a OME model are the weak and strong hadronic vertices. The $\Lambda\pi N$ weak Hamiltonian is given in Eq. (4). For the strong $NN\pi$ Hamiltonian one has the usual pseudoscalar coupling:

$$\mathcal{H}^S_{NN\pi} = ig_{NN\pi}\overline{\psi}_N\gamma_5\vec{\tau}\cdot\vec{\phi}_\pi\psi_N,$$

$g_{NN\pi}$ being the strong coupling constant for the $NN\pi$ vertex. In momentum space, the non–relativistic transition potential in the OPE approximation is then:

$$V_\pi(\vec{q}) = -Gm_\pi^2\frac{g_{NN\pi}}{2m_N}\left(A + \frac{B}{2\bar{m}}\vec{\sigma}_1\cdot\vec{q}\right)\frac{\vec{\sigma}_2\cdot\vec{q}}{\vec{q}^2 + m_\pi^2}\vec{\tau}_1\cdot\vec{\tau}_2,$$

where $\bar{m} = (m_\Lambda + m_N)/2$ and $\vec{q}$ is the momentum of the exchanged pion.

Due to the large momenta ($\simeq 420$ MeV) exchanged in the $\Lambda N \to nN$ transition, the OPE mechanism describes the long range part of the interaction, and more massive mesons are expected to contribute at shorter distances.

Non–trivial difficulties arise with the heavier mesons, since their weak couplings in the ΛN vertex are not known experimentally. For example, if one includes in the calculation the contribution of the ρ–meson, the weak $\Lambda N\rho$ and strong $NN\rho$ Hamiltonians give rise to the following ρ–meson transition potential:

$$V_\rho(\vec{q}) = Gm_\pi^2\left[g_{NN\rho}^V\alpha - \frac{(\alpha + \beta)(g_{NN\rho}^V + g_{NN\rho}^T)}{4m_nm}(\vec{\sigma}_1\times\vec{q})\cdot(\vec{\sigma}_2\times\vec{q})\right.$$
$$\left. +i\frac{\epsilon(g_{NN\rho}^V + g_{NN\rho}^T)}{2m_m}(\vec{\sigma}_1\times\vec{\sigma}_2)\cdot\vec{q}\right]\frac{\vec{\tau}_1\cdot\vec{\tau}_2}{\vec{q}^2 + m_\rho^2},$$

where the weak coupling constants α, β and ϵ must be evaluated theoretically and turn out to be quite model–dependent.

The most general OME potential accounting for the exchange of pseudoscalar and vector mesons can be expressed through the following decomposition:

$$(5) \qquad\qquad V(\vec{r}) = \sum_m V_m(\vec{r}) = \sum_m\sum_\alpha V_m^\alpha(r)\hat{O}^\alpha(\hat{\vec{r}})\hat{I}_m,$$

where $m = \pi$, ρ, K, K^*, ω, η; the spin operators $\hat{O}^\alpha$ are (PV stands for parity–violating):

$$
\hat{O}^\alpha(\hat{\vec{r}}) = \begin{cases}
\hat{1} & \text{central spin–independent,} \\
\vec{\sigma}_1 \cdot \vec{\sigma}_2 & \text{central spin–dependent ,} \\
S_{12}(\hat{\vec{r}}) = 3(\vec{\sigma}_1 \cdot \hat{\vec{r}})(\vec{\sigma}_2 \cdot \hat{\vec{r}}) - \vec{\sigma}_1 \cdot \vec{\sigma}_2 & \text{tensor,} \\
\vec{\sigma}_2 \cdot \hat{\vec{r}} & \text{PV for pseudoscalar mesons,} \\
(\vec{\sigma}_1 \times \vec{\sigma}_2) \cdot \hat{\vec{r}} & \text{PV for vector mesons,}
\end{cases}
$$

whereas the isospin operators $\hat{I}_m$ are:

$$
\hat{I}_m = \begin{cases}
\hat{1} & \text{isoscalars mesons } (\eta,\, \omega), \\
\vec{\tau}_1 \cdot \vec{\tau}_2 & \text{isovector mesons } (\pi,\, \rho), \\
\text{linear combination of } \hat{1} \text{ and } \vec{\tau}_1 \cdot \vec{\tau}_2 & \text{isodoublet mesons } (K,\, K^*).
\end{cases}
$$

For details concerning the potential (5), see Ref. [15, 17].

Assuming the initial hypernucleus to be at rest, the *one–body induced non–mesonic decay rate* can then be written as:

$$
(6) \qquad \Gamma_1 = \int \frac{d\vec{p}_1}{(2\pi)^3} \int \frac{d\vec{p}_2}{(2\pi)^3} \, 2\pi \, \delta(\text{E.C.}) \overline{\sum} \, |\mathcal{M}(\vec{p}_1, \vec{p}_2)|^2 \, ,
$$

where $\delta(\text{E.C.})$ stands for the energy conserving delta function:

$$
\delta(\text{E.C.}) = \delta\left(m_H - E_R - 2m_N - \frac{\vec{p}_1^{\,2}}{2m_N} - \frac{\vec{p}_2^{\,2}}{2m_N} \right) .
$$

Moreover:

$$
\mathcal{M}(\vec{p}_1, \vec{p}_2) \equiv \langle \Psi_R; N(\vec{p}_1) N(\vec{p}_2) | \hat{T}_{\Lambda N \to NN} | \Psi_H \rangle
$$

is the amplitude for the transition of the initial hypernuclear state $|\Psi_H\rangle$ of mass m_H into a final state composed by a residual nucleus $|\Psi_R\rangle$ with energy E_R and an antisymmetrized two nucleon state $|N(\vec{p}_1) N(\vec{p}_2)\rangle$, $\vec{p}_1$ and $\vec{p}_2$ being the nucleon momenta. The sum $\overline{\sum}$ in Eq. (6) indicates an average over the third component of the hypernuclear total spin and a sum over the quantum numbers of the residual system and over the spin and isospin third components of the outgoing nucleons. Customarily, in shell model calculations the weak–coupling scheme is used to describe the hypernuclear wave function $|\Psi_H\rangle$, the nuclear core wave function being obtained through the technique of fractional parentage coefficients [15]. The many–body transition amplitude $\mathcal{M}(\vec{p}_1, \vec{p}_2)$ is then expressed in terms of two–body amplitudes $\langle NN|V|\Lambda N\rangle$ of the OME potential of Eq. (5).

Two merits of the WFM must be remarked:

- Since the Λ decays from an orbital angular momentum $l = 0$ state, in the non–mesonic decay rate one can easily isolate the contributions of neutron– and proton–induced transitions [15], and the Γ_n/Γ_p ratio can be directly evaluated.

- The nN final state interactions and the ΛN correlations (which are absent in an independent particle shell model) can also be implemented in the calculation [15, 17].

3˙3. *Polarization Propagator Method and Local Density Approximation.* – The hypernuclear decay rates can be studied by using the Polarization Propagator Method [22] to evaluate the Λ self–energy inside the nuclear medium. The polarization propagator is conveniently calculated for a homogeneous system (nuclear matter), within the Random Phase Approximation (RPA) and eventually accounting for additional correlations. The calculation can then be extended to finite nuclei via the Local Density Approximation (LDA).

This many–body technique provides a unified picture of the different decay channels and it is equivalent to the WFM [23] (in the sense that it is a semiclassical approximation of the exact quantum mechanical problem). Obviously, for the mesonic rates the WFM is more reliable than the PPM in LDA, since Γ_M is rather sensitive to the shell structure of the hypernucleus. On the other hand, the propagator method in LDA offers the possibility of calculating the hypernuclear decay rates over a broad range of mass numbers, while the WFM is hardly exploitable for medium and heavy hypernuclei.

To calculate the hypernuclear width one needs the imaginary part of the Λ self–energy:

$$(7) \qquad\qquad \Gamma_\Lambda = -2\,\mathrm{Im}\,\Sigma_\Lambda,$$

which, in the non–relativistic limit, reads:

$$(8) \qquad \Sigma_\Lambda(k) = 3i(Gm_\pi^2)^2 \int \frac{d^4q}{(2\pi)^4} \left(S^2 + \frac{P^2}{m_\pi^2}\vec{q}^{\,2} \right) F_\pi^2(q) G_N(k-q) G_\pi(q).$$

The nucleon and pion propagators in nuclear matter are, respectively:

$$(9) \qquad G_N(p) = \frac{\theta(|\,\vec{p}\,| - k_F)}{p_0 - E_N(\vec{p}) - V_N + i\epsilon} + \frac{\theta(k_F - |\,\vec{p}\,|)}{p_0 - E_N(\vec{p}) - V_N - i\epsilon},$$

and:

$$(10) \qquad G_\pi(q) = \frac{1}{q_0^2 - \vec{q}^{\,2} - m_\pi^2 - \Sigma_\pi^*(q)}.$$

The above form of the non–relativistic nucleon propagator refers to a non–interacting Fermi system but includes corrections due to Pauli principle and an average binding. In the previous equations, $p = (p_0, \vec{p})$ and $q = (q_0, \vec{q})$ denote four–vectors, k_F is the Fermi momentum, E_N is the nucleon total free energy, V_N is the nucleon binding energy
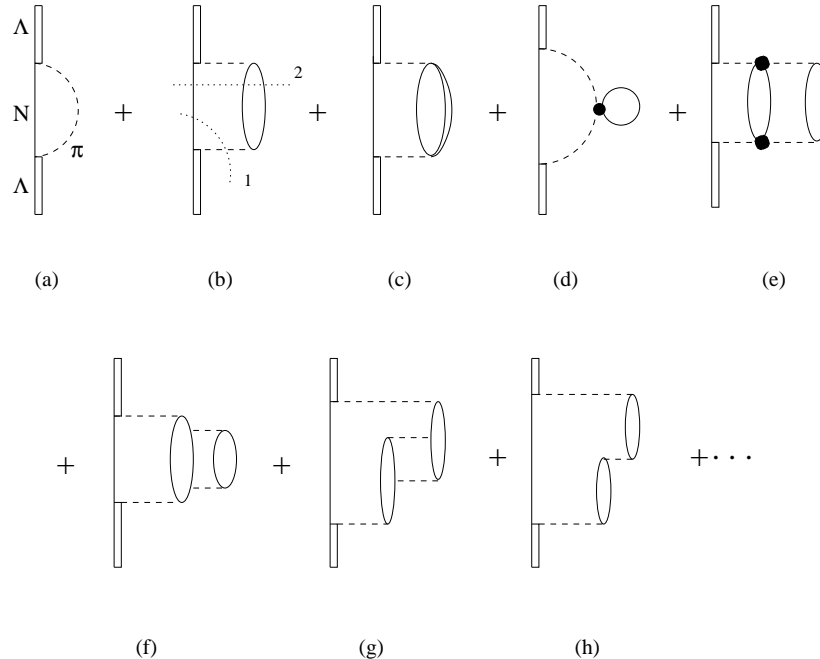
Fig. 3. – Lowest order terms for the Λ self–energy in nuclear matter. The meaning of the various diagrams is explained in the text.

(which is density–dependent), and Σ_π^* is the pion proper self–energy in nuclear matter. This quantity has been carefully evaluated within several many–body frameworks and includes the (strong) coupling of the pion to particle–hole (p–h) states, collective RPA states and more complicated nuclear correlated states (e.g., the two–particle two–hole states). A monopole form factor $F_\pi(q)$ describing the hadronic structure of the $\pi\Lambda N$ vertex is also included in Eq. (8).

We note here that the parity–conserving term ($l = 1$ term) in Eq. (8) contributes only about 12% of the total free decay width. However, the P–wave interaction becomes dominant in the nuclear non–mesonic decay, because of the larger exchanged momenta.

In Fig. 3 we show the lowest order Feynman diagrams for the Λ self–energy in nuclear matter. Diagram (a) represents the bare self–energy term, including the effects of the Pauli principle and of binding on the intermediate nucleon. In (b) and (c) the pion couples to a p–h and a Δ–h pair, respectively. Diagram (d) is an insertion of S–wave pion self–energy at lowest order. In diagram (e) we show a $2p$–$2h$ excitation coupled to the pion through S–wave πN interactions. Other $2p$–$2h$ excitations, coupled in P–wave, are shown in (f) and (g), while (h) is a RPA iteration of diagram (b).

In Eq. (8) there are two different sources of imaginary part. The analytical structure of the integrand allows the integration over q_0 [24]. After performing this integration,

an imaginary part is obtained from the (renormalized) pion–nucleon pole and physically corresponds to the mesonic decay of the hyperon. Moreover, the pion proper self–energy $\Sigma_\pi^*(q)$ has an imaginary part itself for $(q_0, \vec{q})$ values which correspond to the excitation of p–h, Δ–h, $2p$–$2h$, etc states on the mass shell. By expanding the pion propagator $G_\pi(q)$ as in Fig. 3 and integrating Eq. (8) over q_0, the nuclear matter Λ decay width of Eq. (7) becomes [24]:

$$\Gamma_\Lambda(\vec{k}, \rho) = -6(Gm_\pi^2)^2 \int \frac{d\vec{q}}{(2\pi)^3} \theta(|\vec{k} - \vec{q}| - k_F) \theta(k_0 - E_N(\vec{k} - \vec{q}) - V_N)$$

(11) $$\times \mathrm{Im}\left[\alpha(q)\right]_{q_0 = k_0 - E_N(\vec{k} - \vec{q}) - V_N},$$

where:

$$\alpha(q) = \left(S^2 + \frac{P^2}{m_\pi^2} \vec{q}^{\,2}\right) F_\pi^2(q) G_\pi^0(q) + \frac{\tilde{S}^2(q) U_L(q)}{1 - V_L(q) U_L(q)}$$

(12) $$+ \frac{\tilde{P}_L^2(q) U_L(q)}{1 - V_L(q) U_L(q)} + 2 \frac{\tilde{P}_T^2(q) U_T(q)}{1 - V_T(q) U_T(q)}.$$

In Eq. (11) the first θ function forbids intermediate nucleon momenta smaller than the Fermi momentum, while the second one requires the pion energy q_0 to be positive. Moreover, the Λ energy, $k_0 = E_\Lambda(\vec{k}) + V_\Lambda$, contains a phenomenological binding term. With the exception of diagram (a), the pion lines of Fig. 3 have been replaced, in Eq. (12), by the effective interactions $\tilde{S}$, $\tilde{P}_L$, $\tilde{P}_T$, V_L, V_T (L and T stand for spin–longitudinal and spin–transverse, respectively), which include π– and ρ–exchange modulated by the effect of short range repulsive correlations. The potentials V_L and V_T represent the (strong) p–h interaction and include a Landau parameter g', which accounts for the short range repulsion, while $\tilde{S}$, $\tilde{P}_L$ and $\tilde{P}_T$ correspond to the lines connecting weak and strong hadronic vertices and contain another Landau parameter, g'_Λ, which is related to the strong ΛN short range correlations.

Furthermore, in Eq. (12):

$$G_\pi^0(q) = \frac{1}{q_0^2 - \vec{q}^{\,2} - m_\pi^2},$$

is the free pion propagator, while $U_L(q)$ and $U_T(q)$ contain the Lindhard functions for p–h and Δ–h excitations [25] and also account for the irreducible $2p$–$2h$ polarization propagator:

(13) $$U_{L,T}(q) = U^{ph}(q) + U^{\Delta h}(q) + U_{L,T}^{2p2h}(q).$$

They appear in Eq. (12) within the standard RPA expression:

$$\frac{U_{L(T)}(q)}{1 - V_{L(T)}(q) U_{L(T)}(q)} = U_{L(T)}(q) + U_{L(T)}(q) V_{L(T)}(q) U_{L(T)}(q) +$$

(14) $$+ U_{L(T)}(q) V_{L(T)}(q) U_{L(T)}(q) V_{L(T)}(q) U_{L(T)}(q) + \ldots$$

The decay width (11) depends both explicitly and through $U_{L,T}(q)$ on the nuclear matter density $\rho = 2k_F^3/3\pi^2$.

The Lindhard function U^{ph} ($U^{\Delta h}$) is given by:

$$(15) \qquad U^{ph(\Delta h)}(q) = -4i \int \frac{d^4 p}{(2\pi)^3} G_N^0(p) G_{N(\Delta)}^0(p+q),$$

with the *free* nucleon and Delta propagators:

$$(16) \qquad G_N^0(p) = \frac{\theta(|\,\vec{p}\,| - k_F)}{p_0 - T_N(\vec{p}) + i\epsilon} + \frac{\theta(k_F - |\,\vec{p}\,|)}{p_0 - T_N(\vec{p}) - i\epsilon},$$

$$(17) \qquad G_\Delta^0(p) = \frac{4}{9} \frac{1}{p_0 - T_\Delta(\vec{p}) - \delta M_{\Delta N} + i\,\Gamma_\Delta/2},$$

where $T_{N(\Delta)}$ is the nucleon (Delta) kinetic energy, Γ_Δ the free Δ width and $\delta M_{\Delta N} = m_\Delta - m_N$. We remind that $U^{ph}(q)$ and $U^{\Delta h}(q)$ can be analytically evaluated in nuclear matter.

For the evaluation of $U_{L,T}^{2p2h}$ we discuss two different approaches. In Refs. [26, 27] a phenomenological parameterization was adopted: this consists in relating $U_{L,T}^{2p2h}$ to the available phase space for on–shell 2p–2h excitations in order to extrapolate for off–mass shell pions the experimental data of P–wave absorption of real pions in pionic atoms. In an alternative approach [28], $U_{L,T}^{2p2h}$ is evaluated microscopically, starting from a classification of the relevant Feynman diagrams according to the so–called bosonic loop expansion, which is obtained within a functional approach.

We notice here, in connection with Eqs. (8) and (10), that the full (proper) pion self–energy

$$\Sigma_\pi^*(q) = \Sigma_\pi^{(S)*}(q) + \Sigma_\pi^{(P)*}(q),$$

contains a P–wave term, which is related to the spin–longitudinal polarization propagator $U_L(q)$ according to:

$$(18) \qquad \Sigma_\pi^{(P)*}(q) = \frac{\vec{q}^{\,2} \dfrac{f_\pi^2}{m_\pi^2} F_\pi^2(q) U_L(q)}{1 - \dfrac{f_\pi^2}{m_\pi^2} g_L(q) U_L(q)},$$

the Landau function $g_L(q)$ being given in the appendix of Ref. [5]. $\Sigma_\pi^*(q)$ also contains an S–wave term, which, by using the parameterization of Ref. [29], can be written as:

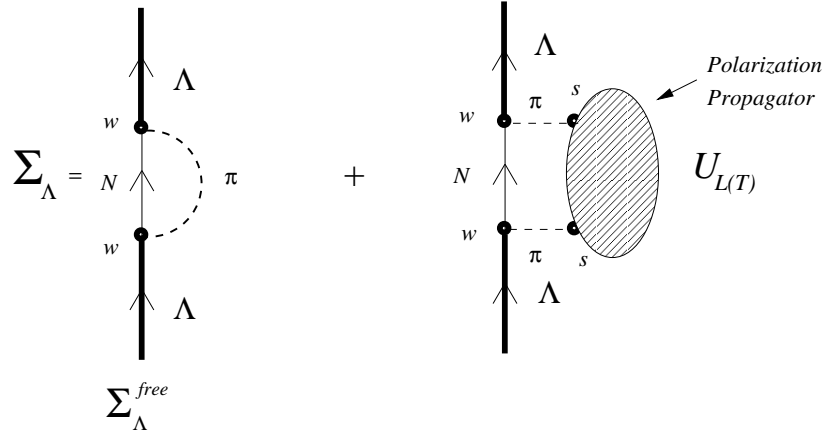$$(19) \qquad \Sigma_\pi^{(S)*}(q) = -4\pi \left(1 + \frac{m_\pi}{m_N}\right) b_0 \rho.$$

Fig. 4. – Schematic representation of the total Λ self-energy in terms of the π–self energy and polarization insertions; in the vertexes $w =$ weak, $s =$ strong.

The parameter b_0 is usually taken from the phenomenology of pionic atoms (see, for example, Ref. [30]). The function $\Sigma_\pi^{(S)\,*}$ is real (constant and positive), therefore it contributes only to the mesonic decay [diagram (d) in Fig. 3 is the relative lowest order]. On the contrary, the P–wave self–energy is complex and attractive: Re $\Sigma_\pi^{(P)\,*}(q) < 0$. It contributes to all the decay channels, in particular to the two–body induced non–mesonic decay width. A schematic picture of the relation between the Λ and π self–energies is illustrated in Fig. 4, where the polarization propagator insertion on the pionic line summarizes all contributions explicitly shown in Fig. 3 and many others, up to infinite order.

The propagator method provides a unified picture of the decay widths. A non–vanishing imaginary part in a self–energy diagram requires placing simultaneously on–shell the particles of the considered intermediate state. For instance, diagram (b) in Fig. 3 has two sources of imaginary part. One comes from cut 1, where the nucleon and the pion are placed on–shell. This term contributes to the mesonic channel: the final pion eventually interacts with the medium through a p–h excitation and then escapes from the nucleus. Diagram (b) and further iterations lead to a renormalization of the pion in the medium which may increase the mesonic rate even by one or two orders of magnitude in heavy nuclei [8, 9, 24]. The cut 2 in Fig. 3(b) places a nucleon and a p–h pair on shell, so it is the lowest order contribution to the physical process $\Lambda N \to nN$. Analogous considerations apply to all the considered diagrams.

A couple of remarks may be useful, here, for those who are not familiar with the language of many–body theory.

1. The one–body induced process $\Lambda N \to nN$ (for example via the exchange of a pion) translates, inside the nuclear medium, into the creation of a particle–hole pair, the
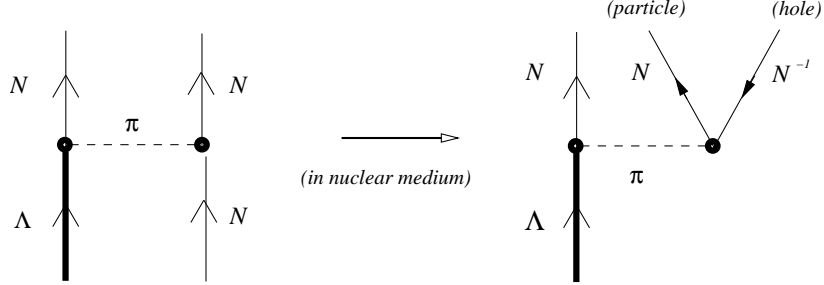
Fig. 5. – One–body induced process in the language of particle–hole states.

hole representing the state of the initial nucleon, which turns out to be vacant, in the medium, after the weak interaction with the Λ. This is schematically illustrated in Fig. 5.

2. The relation between the one–body induced decay width, Γ_1, and the imaginary part of the Λ self–energy, say, of diagram (b) in Fig. 3, is represented in the upper panel of Fig. 6, where the modulus square of the decay amplitude is pictorially related to the Imaginary part of the considered diagram, with a cut putting on–shell the 2 nucleon, 1 hole intermediate state. Analogously, the two–body induced decay width is related to the Imaginary part of diagrams like, e.g., Fig. 3(f), the cut being placed on the 2p–2h intermediate state of the polarization propagator. This is represented in the lower panel of Fig. 6.

In order to evaluate the various contributions to the width stemming from Eq. (11), it is convenient to consider all the intervening free meson propagators as real. Then the imaginary part of (12) will develop the following contributions:

$$(20) \qquad \operatorname{Im} \frac{U_{L,T}(q)}{1 - V_{L,T}(q)U_{L,T}(q)} = \frac{\operatorname{Im} U^{ph}(q) + \operatorname{Im} U^{\Delta h}(q) + \operatorname{Im} U_{L,T}^{2p2h}(q)}{\mid 1 - V_{L,T}(q)U_{L,T}(q) \mid^2}.$$

The three terms in the numerator of Eq. (20) can be interpreted as different decay mechanisms of the hypernucleus. The term proportional to $\operatorname{Im} U^{ph}$ provides the one–nucleon induced non–mesonic rate, Γ_1. There is no overlap between $\operatorname{Im} U^{ph}(q)$ and the pole $q_0 = \omega(\vec{q})$ in the (dressed) pion propagator $G_\pi(q)$: thus the separation of the mesonic and one–body stimulated non–mesonic channels is unambiguous.

Further, $\operatorname{Im} U^{\Delta h}$ accounts for the $\Delta \to \pi N$ decay width, thus representing a (small) contribution to the mesonic decay.

The third contribution of Eq. (20), proportional to $\operatorname{Im} U_{L,T}^{2p2h}$, intervenes in a wide kinematic range, in which the above mentioned cuts put on the mass shell not only the 2p–2h lines, but possibly also the pionic lines. Indeed, the renormalized pion pole in
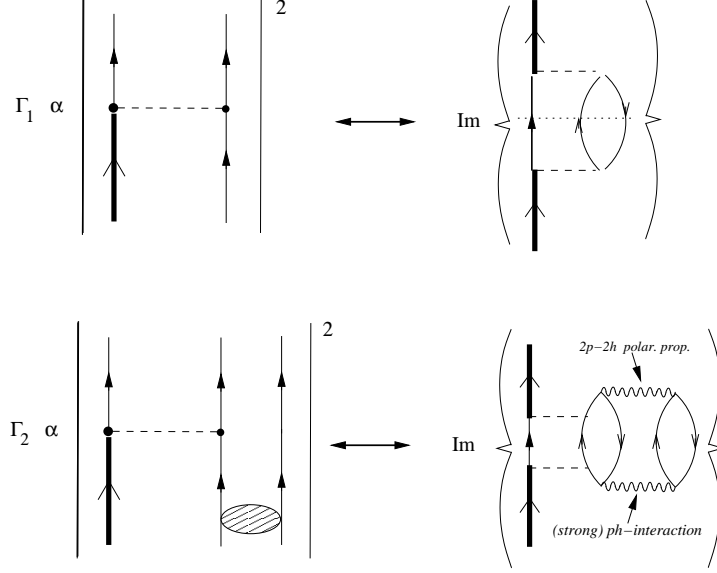
Fig. 6. – Schematic relation between the one-body (upper panel) and two–body (lower panel) Λ decay amplitudes and the Imaginary part of specific contributions to the Λ self-energy.

Eq. (10) is given by the dispersion relation:

$$\omega^2(\vec{q}) - \vec{q}^{\,2} - m_\pi^2 - \mathrm{Re}\,\Sigma_\pi^* \left[\omega(\vec{q}), \vec{q}\,\right] = 0,$$

with the constraint:

$$\omega(\vec{q}) = k_0 - E_N(\vec{k} - \vec{q}) - V_N.$$

At the pion pole, $\mathrm{Im}\,U_{L,T}^{2p2h} \neq 0$, thus the two–body induced non–mesonic width, Γ_2, cannot be disentangled from the mesonic width, Γ_{M}. In other words, part of the decay rate calculated from $\mathrm{Im}\,U_{L,T}^{2p2h}$ is due to the excitations of the renormalized pion and gives in fact Γ_{M}, with the exception of the mesonic contribution originating from $\mathrm{Im}\,U^{\Delta h}$, which is, however, only a small fraction of Γ_{M}.

In order to separate Γ_{M} from Γ_2, in the numerical calculation it is convenient to evaluate the mesonic width by adopting the following prescription. We start from Eq. (11), setting:

$$(21) \qquad \alpha(q) = \alpha_M(q) \equiv \left(S^2 + \frac{P^2}{m_\pi^2}\vec{q}^{\,2} \right) F_\pi^2(q) G_\pi(q),$$

and omitting $\mathrm{Im}\,\Sigma_\pi^*$ in G_π (which corresponds to assume $\mathrm{Im}\,U^{ph} = \mathrm{Im}\,U^{\Delta h} = \mathrm{Im}\,U_{L,T}^{2p2h} =$

0). Then $\operatorname{Im} \alpha_M(q)$ only accounts for the (real) contribution of the pion pole:

$$\operatorname{Im} G_\pi(q) = -\pi\delta\left[q_0^2 - \vec{q}^{\,2} - m_\pi^2 - \operatorname{Re}\Sigma_\pi^*(q)\right].$$

Once the mesonic decay rate is known, one can calculate the three–body non–mesonic rate by subtracting Γ_M and Γ_1 from the total rate Γ_T, which one gets via the full expression for $\alpha(q)$ [Eq. (12)].

Using the PPM, the decay widths of finite nuclei can be obtained from the ones evaluated in nuclear matter via the LDA: in this approach the Fermi momentum is made r–dependent (namely a local Fermi sea of nucleons is introduced) and related to the nuclear density by the same relation which holds in nuclear matter:

$$(22) \qquad k_F(\vec{r}) = \left\{\frac{3}{2}\pi^2\rho(\vec{r})\right\}^{1/3}.$$

More specifically, one usually assumes the nuclear density to be a Fermi distribution:

$$\rho_A(r) = \frac{\rho_0}{\left\{1 + \exp\left[\dfrac{r - R(A)}{a}\right]\right\}}$$

with $R(A) = 1.12A^{1/3} - 0.86A^{-1/3}$ fm, $a = 0.52$ fm and $\rho_0 = A\left\{\frac{4}{3}\pi R^3(A)\left(1 + \left[\frac{\pi a}{R(A)}\right]^2\right)\right\}^{-1}$.

Moreover, the nucleon binding potential V_N also becomes r–dependent in LDA. In Thomas–Fermi approximation one assumes:

$$\epsilon_F(\vec{r}) + V_N(\vec{r}) \equiv \frac{k_F^2(\vec{r})}{2m_N} + V_N(\vec{r}) = 0.$$

With these prescriptions one can then evaluate the decay width in finite nuclei by using the semiclassical approximation, through the relation:

$$(23) \qquad \Gamma_\Lambda(\vec{k}) = \int d\vec{r}\,|\psi_\Lambda(\vec{r})|^2\Gamma_\Lambda\left[\vec{k}, \rho(\vec{r})\right],$$

where ψ_Λ is the appropriate Λ wave function and $\Gamma_\Lambda[\vec{k}, \rho(\vec{r})]$ is given by Eqs. (11), (12) with a position dependent nuclear density. This decay rate can be regarded as the $\vec{k}$–component of the Λ decay rate in the nucleus with density $\rho(\vec{r})$. It can be used to estimate the decay rates by averaging over the Λ momentum distribution $|\tilde{\psi}_\Lambda(\vec{k})|^2$. One then obtains the following total width:

$$(24) \qquad \Gamma_T = \int d\vec{k}\,|\tilde{\psi}_\Lambda(\vec{k})|^2\Gamma_\Lambda(\vec{k}),$$

which can be compared with the experimental results.

3˙3.1. *Phenomenological 2p–2h propagator.* Coming to the phenomenological evaluation of the *2p–2h* contributions in the Λ self–energy, the momentum dependence of the imaginary part of $U^{2p2h}_{L,T}$ can be obtained from the available phase space, through the following equation [26]:

$$(25) \qquad \operatorname{Im} U^{2p2h}_{L,T}(q_0, \vec{q}; \rho) = \frac{P(q_0, \vec{q}; \rho)}{P(m_\pi, \vec{0}; \rho_{\text{eff}})} \operatorname{Im} U^{2p2h}_{L,T}(m_\pi, \vec{0}; \rho_{\text{eff}}),$$

where $\rho_{\text{eff}} = 0.75\rho$. By neglecting the energy and momentum dependence of the *p–h* interaction, the phase space available for on–shell *2p–2h* excitations [calculated, for simplicity, from diagram 3(e)] at energy–momentum $(q_0, \vec{q})$ and density ρ turns out to be:

$$P(q_0, \vec{q}; \rho) \propto \int \frac{d^4k}{(2\pi)^4} \operatorname{Im} U^{ph}\left(\frac{q}{2} + k; \rho\right) \operatorname{Im} U^{ph}\left(\frac{q}{2} - k; \rho\right)$$
$$\times \theta\left(\frac{q_0}{2} + k_0\right) \theta\left(\frac{q_0}{2} - k_0\right).$$

In the region of $(q_0, \vec{q})$ where the *p–h* and Δ–*h* excitations are off–shell, the relation between U^{2p2h}_L and the *P*–wave pion–nucleus optical potential V_{opt} is given by [see also Eq. (18), in the language of pion self–energy]:

$$(26) \qquad \frac{\vec{q}^2 \dfrac{f_\pi^2}{m_\pi^2} F_\pi^2(q) U^{2p2h}_L(q)}{1 - \dfrac{f_\pi^2}{m_\pi^2} g_L(q) U_L(q)} = 2q_0 V_{\text{opt}}(q).$$

At the pion threshold V_{opt} is usually parameterized as:

$$(27) \qquad 2q_0 V_{\text{opt}}(q_0 \simeq m_\pi, \vec{q} \simeq \vec{0}; \rho) = -4\pi \vec{q}^2 \rho^2 C_0,$$

where C_0 is a complex number which can be extracted from experimental data on pionic atoms. By combining Eqs. (26) and (27) it is possible to parameterize the proper *2p–2h* excitations in the spin–longitudinal channel through Eq. (25), by setting:

$$(28) \qquad \vec{q}^2 \frac{f_\pi^2}{m_\pi^2} F_\pi^2(q_0 \simeq m_\pi, \vec{q} \simeq \vec{0}) U^{2p2h}_L(q_0 \simeq m_\pi, \vec{q} \simeq \vec{0}; \rho) = -4\pi \vec{q}^2 \rho^2 C_0^*.$$

The relation between C_0 and C_0^* is fixed on the basis of the same RPA expression for the polarization propagator contained in Eq. (26); hence the value of C_0^* also depends on the correlation function g_L. From the analysis of pionic atoms data made in Ref. [31] and taking $g' \equiv g_L(0) = 0.615$, one obtains:

$$C_0^* = (0.105 + i0.096)/m_\pi^6.$$

The spin–transverse component of U^{2p2h} is assumed to be equal to the spin–longitudinal one, $U_T^{2p2h} = U_L^{2p2h}$, and the real parts of U_L^{2p2h} and U_T^{2p2h} are considered constant [by using Eq. (28)] because they are not expected to be too sensitive to variations of q_0 and $\vec{q}$. The assumption $U_T^{2p2h} = U_L^{2p2h}$ is not *a priori* a good approximation, but it is the only one which can be employed in the present phenomenological description. Yet, the differences between U_L^{2p2h} and U_T^{2p2h} can only mildly change the partial decay widths [5]: in fact, $U_{L,T}^{2p2h}$ are summed to U^{ph}, which gives the dominant contribution. Moreover, for $U_L^{2p2h} = U_T^{2p2h}$ the transverse contribution to Γ_2 [fourth term in the right hand side of Eq. (12)] is only about 16% of Γ_2 (namely $2 \div 3\%$ of the total width) in medium–heavy hypernuclei.

The simplified form of the phenomenological *2p–2h* propagator, together with the availability of analytical expressions for U^{ph} and $U^{\Delta-h}$, makes this approach particularly suitable for employing the above mentioned LDA.

3˙3.2. *Functional approach to the Λ self–energy.* In alternative to the above mentioned phenomenological approach for the two–body induced decay width, we briefly discuss here a truly microscopic approach. Indeed the most relevant Feynman diagrams for the calculation of the Λ self–energy can be obtained in the framework of a functional method: following Ref. [28], one can derive a classification of the diagrams according to the prescription of the so–called bosonic loop expansion.

The functional techniques can provide a theoretically founded derivation of new classes of Feynmann diagram expansions in terms of powers of suitably chosen parameters. For example, the already mentioned ring approximation (a subclass of RPA) automatically appears in this framework at the mean field level. This method has been extensively applied to the analysis of different processes in nuclear physics [32–34]. Here it is employed for the calculation of the Λ self–energy in nuclear matter, which can be expressed through the nuclear responses to pseudoscalar–isovector and vector–isovector fields. The polarization propagators obtained in this framework include ring–dressed meson propagators and almost the whole spectrum of *2p–2h* excitations (expressed in terms of a one–loop expansion with respect to the ring–dressed meson propagators), which are required for the evaluation of Γ_2.

Let us first consider the polarization propagator in the pionic (spin–longitudinal) channel. To illustrate the procedure, it is useful to start from a Lagrangian describing a system of nucleons interacting with pions through a pseudoscalar–isovector coupling:

$$(29) \qquad \mathcal{L}_{\pi N} = \overline{\psi}(i\slashed{\partial} - m_N)\psi + \frac{1}{2}\partial_\mu \vec{\phi} \cdot \partial^\mu \vec{\phi} - \frac{1}{2}m_\pi^2 \vec{\phi}^{\,2} - i\overline{\psi}\vec{\Gamma}\psi \cdot \vec{\phi},$$

where ψ $(\vec{\phi})$ is the nucleonic (pionic) field and $\vec{\Gamma} = g\gamma_5\vec{\tau}$ $(g = 2f_\pi m_N/m_\pi)$ is the spin–isospin matrix in the spin–longitudinal isovector channel. We remind the reader that in the calculation of the hypernuclear decay rates one also needs the polarization propagator in the transverse channel [see Eqs. (11) and (12)]: hence, one has to include in the model other mesonic degrees of freedom, like the ρ meson. Since the bosonic loop expansion is

characterized by the topology of the diagrams, this is relatively straightforward and the same scheme can be easily applied to mesonic fields other than the pionic one.

The generating functional, expressed in terms of Feynman path integrals, associated with the Lagrangian (29) has the form:

$$(30) \qquad Z[\vec{\varphi}] = \int \mathcal{D}\left[\overline{\psi}, \psi, \vec{\phi}\right] \exp\left\{i \int dx \left[\mathcal{L}_{\pi N}(x) - i\overline{\psi}(x)\vec{\Gamma}\psi(x) \cdot \vec{\varphi}(x)\right]\right\},$$

where a *classical* external field $\vec{\varphi}$ with the quantum numbers of the pion has been introduced (here and in the following the coordinate integrals are 4–dimensional). All the fields in the functional integrals have to be considered as classical variables, but with the correct commuting properties (hence the fermionic fields are Grassman variables).

The physical quantities of interest for the problem are then deduced from the generating functional by means of functional differentiations. In particular, by introducing a new functional Z_c such that:

$$(31) \qquad\qquad\qquad Z[\vec{\varphi}] = \exp\left\{iZ_c[\vec{\varphi}]\right\},$$

the spin–longitudinal, isovector polarization propagator turns out to be the second functional derivative of Z_c with respect to the source $\vec{\varphi}$ of the pionic field:

$$(32) \qquad\qquad\qquad \Pi_{ij}(x, y) = -\left[\frac{\delta^2 Z_c[\vec{\varphi}]}{\delta\varphi_i(x)\delta\varphi_j(y)}\right]_{\vec{\varphi}=0}.$$

We note that the use of Z_c instead of Z in Eq. (32) amounts to cancel the disconnected diagrams of the corresponding perturbative expansion (linked cluster theorem). From the generating functional Z one can obtain different approximation schemes according to the order in which the functional integrations are performed.

For the present purpose, it is convenient to integrate Eq. (30) over the nucleonic degrees of freedom *first*. Introducing the change of variable $\vec{\phi} \to \vec{\phi} - \vec{\varphi}$ one obtains:

$$(33) \qquad Z[\vec{\varphi}] = \exp\left\{\frac{i}{2}\int dx\, dy\, \vec{\varphi}(x) \cdot G_\pi^{0^{-1}}(x-y)\vec{\varphi}(y)\right\}$$

$$\times \int \mathcal{D}\left[\overline{\psi}, \psi, \vec{\phi}\right] \exp\left\{i \int dx\, dy\ \left[\overline{\psi}(x)G_N^{-1}(x-y)\psi(y)\right.\right.$$

$$\left.\left. +\frac{1}{2}\vec{\phi}(x) \cdot G_\pi^{0^{-1}}(x-y)\left(\vec{\phi}(y) + 2\vec{\varphi}(y)\right)\right]\right\},$$

where the integral over $\left[\overline{\psi}, \psi\right]$ is gaussian:

$$\int \mathcal{D}\left[\overline{\psi}, \psi\right] \exp\left\{i \int dx\, dy\, \overline{\psi}(x)G_N^{-1}(x-y)\psi(y)\right\} = (\det G_N)^{-1}.$$

Hence, after multiplying Eq. (33) by the unessential factor $\det G_N^0$ (G_N^0 being the free nucleon propagator), which only redefines the normalization constant of the generating functional, and using the property $\det X = \exp\{\mathrm{Tr}\ln X\}$, one obtains:

$$(34) \qquad Z[\vec{\varphi}] = \exp\left\{\frac{i}{2}\int dx\,dy\,\vec{\varphi}(x)\cdot G_\pi^{0^{-1}}(x-y)\vec{\varphi}(y)\right\}$$
$$\times \int \mathcal{D}\left[\vec{\phi}\right]\exp\left\{iS_{\text{eff}}^B\left[\vec{\phi}\right]\right\}.$$

In this expression we have introduced the *bosonic effective action*:

$$(35)\qquad S_{\text{eff}}^B\left[\vec{\phi}\right] = \int dx\,dy\,\left\{\frac{1}{2}\vec{\phi}(x)\cdot G_\pi^{0^{-1}}(x-y)\left[\vec{\phi}(y) + 2\vec{\varphi}(y)\right] + V_\pi\left[\vec{\phi}\right]\right\},$$

where(^{2}):

$$(36)\quad V_\pi\left[\vec{\phi}\right] = i\mathrm{Tr}\sum_{n=1}^{\infty}\frac{1}{n}\left(i\vec{\Gamma}\cdot\vec{\phi}G_N^0\right)^n$$
$$= \frac{1}{2}\sum_{i,j}\mathrm{Tr}\left(\Gamma_i\Gamma_j\right)\int dx\,dy\,\Pi^0(x,y)\phi_i(x)\phi_j(y)$$
$$+ \frac{1}{3}\sum_{i,j,k}\mathrm{Tr}\left(\Gamma_i\Gamma_j\Gamma_k\right)\int dx\,dy\,dz\,\Pi^0(x,y,z)\phi_i(x)\phi_j(y)\phi_k(z) + \mathcal{O}(\vec{\phi}^4).$$

and:

$$(37)\qquad -i\Pi^0(x,y) = iG_N^0(x-y)iG_N^0(y-x),$$
$$(38)\qquad -i\Pi^0(x,y,z) = iG_N^0(x-y)iG_N^0(y-z)iG_N^0(z-x),\ \ \text{etc.}$$

The bosonic effective action (35) contains a term for the free pion field and also a highly non–local pion self–interaction V_π. This effective interaction is given by the sum of all diagrams containing one closed fermion loop and an arbitrary number of pionic legs. We note that the function in Eq. (37) is the free particle–hole polarization propagator. Moreover, the functions $\Pi^0(x,y,\ldots,z)$ are symmetric for cyclic permutations of the arguments.

The next step is the evaluation of the functional integral over the bosonic degrees of freedom in Eq. (34). A perturbative approach to the bosonic effective action (35) does

---

(^{2}) Eq. (36) is a compact writing: for example, the $n=2$ term must be interpreted as:

$$\frac{i}{2}\mathrm{Tr}\left(i\vec{\Gamma}\cdot\vec{\phi}G_N^0\right)^2 = \frac{i}{2}\int dx\,dy\,\mathrm{Tr}\sum_{i,j}i\Gamma_iG_N^0(x-y)\,i\Gamma_jG_N^0(y-x)\phi_i(x)\phi_j(y),$$

where the trace in the right hand side acts on the vertices $\vec{\Gamma}$, and so on.

not seem to provide any valuable results within the capabilities of the present computing tools and in Ref. [28] another approximation scheme, the semiclassical method, was followed.

The lowest order of the semiclassical expansion is the stationary phase approximation (also called saddle point approximation in the Euclidean space): the bosonic effective action is required to be stationary with respect to arbitrary variations of the fields ϕ_i:

$$\frac{\delta S_{\text{eff}}^B \left[\vec{\phi}\right]}{\delta \phi_i(x)} = 0.$$

From the partial derivative of Eq. (35) one obtains the following equation of motion for the classical field $\vec{\phi}$:

$$(39) \qquad \left(\Box + m_\pi^2\right) \phi_i(x) = \int dy \, G_\pi^{0^{-1}}(x-y)\varphi_i(y) + \frac{\delta V_\pi \left[\vec{\phi}\right]}{\delta \phi_i(x)},$$

whose solutions are functional of the external source $\vec{\varphi}$.

It can be shown that in the saddle point approximation the polarization propagator coincides with the well known ring expression:

$$\Pi_{ij}(x,y) = \delta_{ij} \left[\Pi^0(x,y) + \text{Tr}\left(\Gamma_i^2\right) \int du \, dv \, \Pi^0(x,u) G_\pi^{\text{ring}}(u-v)\Pi^0(v,y)\right]$$

$$\equiv \delta_{ij}\Pi^{\text{ring}}(x,y),$$

where:

$$G_\pi^{\text{ring}} = \frac{G_\pi^0}{1 - \text{Tr}\left(\Gamma_i^2\right) G_\pi^0 \Pi^0}$$

is the ring–dressed pion propagator. Hence, the ring approximation corresponds to the mean field level of the present effective theory.

In the next step of the semiclassical method, the bosonic effective action is expanded around the mean field solution:

$$S_{\text{eff}}^B \left[\vec{\phi}\right] = S_{\text{eff}}^B \left[\vec{\phi}^0\right] + \frac{1}{2}\sum_{ij} \int dx \, dy \left[\frac{\delta^2 S_{\text{eff}}^B \left[\vec{\phi}\right]}{\delta \phi_i(x)\delta \phi_j(y)}\right]_{\vec{\phi}=\vec{\phi}^0}$$

$$\times \left[\phi_i(x) - \phi_i^0(x)\right]\left[\phi_j(y) - \phi_j^0(y)\right].$$

Then, after performing the gaussian integration over $\vec{\phi}$, the generating functional (34) [up to an uninteresting normalization factor] reads:

$$(40) \qquad Z\left[\vec{\varphi}\right] = \exp\left\{iS_{\text{eff}}^B \left[\vec{\phi}^0\right] - \frac{1}{2}\text{Tr}\ln\left[\frac{\delta^2 S_{\text{eff}}^B \left[\vec{\phi}\right]}{\delta \phi_i(x)\delta \phi_j(y)}\right]_{\vec{\phi}=\vec{\phi}^0}\right\}.$$
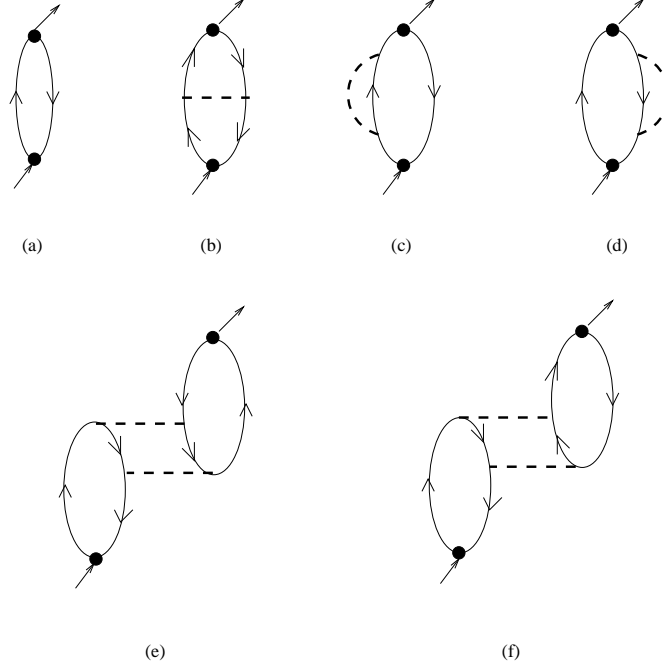
Fig. 7. – Feynman diagrams for the polarization propagator of Eq. (41): (a) particle–hole;
(b) exchange; (c) and (d) self–energy–type; (e) and (f) correlation diagrams. Only the first
contribution to the ring expansion has been drawn. The dashed lines represent ring–dressed
pion propagators.

Lengthy but straightforward calculations [28] lead then to the following total polarization
propagator:

$$(41) \qquad \Pi_{ij}(x,y) = \delta_{ij} \left[\Pi^{\mathrm{ring}}(x,y) + \Pi^{\mathrm{OBL}}(x,y) \right],$$

where:

$$\Pi^{\mathrm{OBL}}(x,y) = \sum_{kl} \mathrm{Tr}\,(\Gamma_k \Gamma_l) \int du\, dv\, G_\pi^{\mathrm{ring}}(u-v) \Pi^0(x,u,y,v)$$

$$+ \sum_{kl} \mathrm{Tr}\,(\Gamma_k \Gamma_l) \int du\, dv\, G_\pi^{\mathrm{ring}}(u-v) \left[\Pi^0(x,u,v,y) + \Pi^0(x,y,v,u) \right]$$

$$+ \int du\, dv\, dw\, ds\, G_\pi^{\mathrm{ring}}(u-w) G_\pi^{\mathrm{ring}}(v-s) \Pi^0(x,u,v)$$

$$(42) \qquad \times \sum_{klmn} \left[\mathrm{Tr}\,(\Gamma_k \Gamma_l \Gamma_m \Gamma_n)\, \Pi^0(y,w,s) + \mathrm{Tr}\,(\Gamma_k \Gamma_l \Gamma_n \Gamma_m)\, \Pi^0(y,s,w) \right].$$

The Feynman diagrams corresponding to Eqs. (41) and (42) are depicted in Fig. 7.

Diagram (a) represents the Lindhard function $\Pi^0(x,y)$, which is just the first term of $\Pi^{\text{ring}}(x,y)$. In (b) we have an *exchange* diagram (the thick dashed lines representing *ring–dressed pion propagators*); (c) and (d) are *self–energy* diagrams, while in (e) and (f) we show the *correlation* diagrams of the present approach. The approximation scheme discussed here is also referred to as bosonic loop expansion (BLE). The practical rule to classify the Feynman diagrams according to their order in the BLE is to reduce to a point all its fermionic lines and to count the number of bosonic loops left out. In this case the diagrams (b)–(f) of Fig. 7, which correspond to Π^{OBL} Eq. (42), reduce to a one–boson–loop (OBL).

The polarization propagator of Eq. (42) is the central result of the present microscopic approach and it has been used [28] for the calculation of the Λ decay width in nuclear matter. Note that the model can easily include the excitation of baryonic resonances, by replacing the fermionic field with multiplets. The topology of the diagrams remains the same as in Fig. 7 but, introducing for example the Δ resonance, each fermionic line represents either a nucleon or a Δ, taking care of isospin conservation. Obviously this procedure substantially increases the number of diagrams.

Moreover, being the BLE characterized by the topology of the diagrams, additional mesonic degrees of freedom together with phenomenological short range correlations can be included by changing the definition of the vertices Γ_i in Eq. (42). In particular, the formalism can be applied to evaluate the functions $U_{L,T}$ of Eq. (13), which are required in Eqs. (11), (12). In the OBL approximation of Eq. (41) and Fig. 7 one has to replace Eq. (12) with:

$$
(43) \qquad \alpha(q) = \left(S^2 + \frac{P^2}{m_\pi^2} \vec{q}^{\,2} \right) F_\pi^2(q) G_\pi^0(q) + \frac{\tilde{S}^2(q) U_1(q)}{1 - V_L(q) U_1(q)}
$$
$$
+ \frac{\tilde{P}_L^2(q) U_1(q)}{1 - V_L(q) U_1(q)} + 2 \frac{\tilde{P}_T^2(q) U_1(q)}{1 - V_T(q) U_1(q)}
$$
$$
+ \left[\tilde{S}^2(q) + \tilde{P}_L^2(q) \right] U_L^{\text{OBL}}(q) + 2 \tilde{P}_T^2(q) U_T^{\text{OBL}}(q),
$$

where

$$
U_1 = U^{ph} + U^{\Delta h},
$$

while $U_{L,T}^{\text{OBL}}$ are evaluated from the diagrams 7(b)–7(f) using the standard Feynman rules. The normalization of these functions is such that $U^{ph}(x,y) = 4\Pi^0(x,y)$, Π^0 being given by Eq. (37). One relevant difference between the OBL formula (43) and the RPA expression of Eq. (12) lies in the fact that in the former, to be consistent with Eq. (42), the *2p–2h* diagrams (which contribute to $U_{L,T}^{\text{OBL}}$) are not RPA–iterated.

4. – Theory versus Experiment

In this Section the predictions of different theoretical models for the total mesonic and non–mesonic weak decay rates are compared with experimental data. We mainly

TABLE I. – *Sensitivity of the decay rates to the Λ wave function for $^{12}_{\Lambda}C$.*

	Micr.	Dover W–S	H.O.	New W–S	BNL [37]	KEK [38]	KEK New [39–41]
Γ_M	0.25	0.25	0.26	0.25	0.11 ± 0.27	0.36 ± 0.13	0.31 ± 0.07
Γ_1	0.69	0.77	0.78	0.82			
Γ_2	0.13	0.15	0.15	0.16			
Γ_{NM}	0.81	0.92	0.93	0.98	1.14 ± 0.20	0.89 ± 0.18	0.83 ± 0.09
Γ_T	1.06	1.17	1.19	1.23	1.25 ± 0.18	1.25 ± 0.18	1.14 ± 0.08

refer to recent works. For a more specialized discussion of theoretical and experimental results see Ref. [5].

4'1. *Phenomenological approach.* – We illustrate here the results which have been obtained for the decay rates by employing the PPM in the phenomenological approach.

In order to evaluate the widths from Eqs. (23), (24), one needs to specify the wave function for the Λ. In Ref. [27] it has been obtained from a Woods–Saxon Λ–nucleus potential with fixed diffuseness $a = 0.6$ fm and with radius and depth such that it exactly reproduces the first two single particle eigenvalues (s and p Λ–levels) of the hypernucleus under analysis.

A crucial ingredient of the calculation is the short range part of the strong NN and ΛN interactions, V_L, V_T, $\tilde{S}$, $\tilde{P}_L$ and $\tilde{P}_T$ entering Eq. (12). They are expressed by the functions $g_{L,T}(q)$ and $g^{\Lambda}_{L,T}(q)$ reported in the appendix of Ref. [5] and contain the Landau parameters g' and g'_{Λ}, respectively. No experimental information is available on g'_{Λ}, while many constraints have been set on g', for example by the well known quenching of the Gamow–Teller resonance. Realistic values of g' within the framework of the ring approximation are in the range $0.6 \div 0.7$ [22]. However, in the present context g' correlates not only p–h pairs but also p–h with $2p$–$2h$ states. Accordingly, the correlation parameters have been fixed to $g' = 0.8$ and $g'_{\Lambda} = 0.4$ [27] in order to reproduce the non–mesonic width measured for $^{12}_{\Lambda}C$.

Using these values for the Landau parameters, we illustrate in Table I the sensitivity of the calculation to the Λ wave function in $^{12}_{\Lambda}C$. In addition to the Woods–Saxon potential (New W–S) that reproduces the s and p Λ–levels, other choices have been introduced: an harmonic oscillator wave function (H.O.) with an "empirical" frequency ω, obtained from the $s - p$ energy shift, the Woods–Saxon wave function of Ref. [35] (Dover W–S) and the microscopic wave function (Micr.) calculated, in Ref. [36], from a non–local self–energy using a realistic ΛN interaction. The results (in units of the free Λ width) are compared with the experimental data from BNL and KEK. By construction, the chosen g' and g'_{Λ} reproduce the experimental non–mesonic width using the W–S wave function which gives the right s and p hyperon levels in $^{12}_{\Lambda}C$. We note that it is possible to generate

Table II. – *Mass dependence of the hypernuclear weak decay rates (taken from Ref. [5]).*

$^{A+1}_{\Lambda}Z$	Γ_M	Γ_1	Γ_2	Γ_T
$^{5}_{\Lambda}$He	0.60	0.27	0.04	0.91
$^{12}_{\Lambda}$C	0.25	0.82	0.16	1.23
$^{28}_{\Lambda}$Si	0.07	1.02	0.21	1.30
$^{40}_{\Lambda}$Ca	0.03	1.05	0.21	1.29
$^{56}_{\Lambda}$Fe	0.01	1.12	0.21	1.35
$^{89}_{\Lambda}$Y	6×10^{-3}	1.16	0.22	1.38
$^{139}_{\Lambda}$La	6×10^{-3}	1.14	0.18	1.33
$^{208}_{\Lambda}$Pb	1×10^{-4}	1.21	0.19	1.40

the microscopic wave function of Ref. [36] for carbon via a local hyperon–nucleus W–S potential with radius $R = 2.92$ fm and depth $V_0 = -23$ MeV. Although this potential reproduces fairly well the experimental s–level for the Λ in $^{12}_{\Lambda}$C, it does not reproduce the p–level. A completely phenomenological Λ–nucleus potential, that can easily be extended to heavier nuclei and reproduces the experimental Λ single particle levels as well as possible, has been preferably adopted in Ref. [27]: the potential parameters obtained for carbon are $R = 2.27$ fm and $V_0 = -32$ MeV.

To analyze the results of Table I, we note that the microscopic wave function is substantially more extended than all the other wave functions. The Dover's parameters [35], namely $R = 2.71$ fm and $V_0 = -28$ MeV, give rise to a Λ wave function that is somewhat more extended than the New W–S one but is very similar to the one obtained from a harmonic oscillator with an empirical frequency $\hbar\omega = 10.9$ MeV. Consequently, the non–mesonic width from the Dover's wave function is very similar to the one obtained from the harmonic oscillator and slightly smaller than the new W–S one. The microscopic wave–function predicts the smallest non–mesonic widths due to the more extended Λ wave–function, which explores regions of lower density, where the probability of interacting with one or more nucleons is smaller. From Table I one can also see that, against intuition, the mesonic width is quite insensitive to the Λ wave function: the different choices give rise to total decay widths which may differ at most by 15%.

Using the New W–S wave functions and the Landau parameters $g' = 0.8$ and $g'_\Lambda = 0.4$, in Refs. [5, 27] the calculation has been extended to hypernuclei from $^{5}_{\Lambda}$He to $^{208}_{\Lambda}$Pb. Notice that, in order to reproduce the experimental s and p levels for the hyperon in the different nuclei one must use potentials with nearly constant depth, around $28 \div 32$ MeV, in all but the lightest hypernucleus ($^{5}_{\Lambda}$He). For this hypernucleus the Λ–nucleus mean potential has a repulsive core and the most convenient Λ wave function turns out to be the one derived in Ref. [42] within a quark model description of $^{5}_{\Lambda}$He.

Table II shows the resulting hypernuclear decay rates in units of the free Λ width. We observe that the mesonic rate rapidly vanishes by increasing the nuclear mass number A.

This is well known and it is related to the decreasing phase space allowed for the mesonic channel, and to smaller overlaps between the Λ wave function and the nuclear surface, as A increases. In Fig. 8 the results of Ref. [5, 27] for Γ_{M} are compared with the ones of Nieves–Oset [8] and Motoba–Itonaga–Bandō [9, 43], which were obtained within a shell model framework. Also the central values of the available experimental data are shown. Although the WFM is more reliable than the LDA for the evaluation of the mesonic rates (since the small energies involved in the decay amplify the effects of the nuclear shell structure), one sees that the LDA calculation of Ref. [27] fairly agrees with the WFM ones and with the data. In particular, Table II shows that the results for $^{12}_{\Lambda}$C and $^{28}_{\Lambda}$Si are in agreement with the very recent KEK measurements [41]: $\Gamma_{\mathrm{M}}(^{12}_{\Lambda}\mathrm{C})/\Gamma^{\mathrm{free}}_{\Lambda} = 0.31 \pm 0.07$, $\Gamma_{\pi^-}(^{28}_{\Lambda}\mathrm{Si})/\Gamma^{\mathrm{free}}_{\Lambda} = 0.046 \pm 0.011$. The results for $^{40}_{\Lambda}$Ca, $^{56}_{\Lambda}$Fe and $^{89}_{\Lambda}$Y are in agreement with the old emulsion data (quoted in Ref. [12]), which indicates $\Gamma_{\pi^-}/\Gamma_{\mathrm{NM}} \simeq (0.5 \div 1) \times 10^{-2}$ in the region $40 < A < 100$. Moreover, the recent KEK experiments [41] obtained the limit: $\Gamma_{\pi^-}(^{56}_{\Lambda}\mathrm{Fe})/\Gamma^{\mathrm{free}}_{\Lambda} < 0.015$ (90% CL). It is worth noticing, in figure 8, the rather pronounced oscillations of Γ_{M} in the calculation of Refs. [9, 43], which are caused by shell effects.

As a final comment to Table II, we note that, with the exception of $^{5}_{\Lambda}$He, the two–body induced decay is rather independent of the hypernuclear dimension and it is about 15% of the total width. Previous works [26, 44] gave more emphasis to this new channel, without, however, reproducing the experimental non–mesonic rates. The total width does not change much with A, as it is also shown by the experiment.

In Fig. 9 the results of Table II are compared with recent (after 1990) experimental data for Γ_{NM} and Γ_{T}. The theoretical results are in good agreement with the data over the whole hypernuclear mass range explored. The saturation of the $\Lambda N \rightarrow nN$ interaction in nuclei is well reproduced.

4˙2. *Microscopic approach*. – The results discussed in this subsection have been obtained by applying the one–boson–loop formalism developed in Section **3**˙3.2 for nuclear matter. Although, in principle, one could extend this calculation to finite nuclei through the local density approximation, in practice this would require prohibitive computing times. Indeed, the latter are already quite conspicuous for the evaluation of the diagrams of Fig. 7 at *fixed* Fermi momentum. Hence, in order to compare the results with the experimental data in finite nuclei, different Fermi momenta have been employed in the nuclear matter calculation. The average, fixed Fermi momentum, which is appropriate for the present purposes, has been obtained by weighting each local Fermi momentum $k^A_F(r)$ with the probability density of the hyperon in the considered nucleus:

$$(44) \qquad\qquad \langle k_F \rangle_A = \int d\vec{r}\, k^A_F(\vec{r})|\psi_\Lambda(\vec{r})|^2.$$

It is then possible to classify the hypernuclei for which experimental data on the non–mesonic decay rate are available into three mass regions (medium–light: $A \simeq 10$; medium: $A \simeq 30 \div 60$; and heavy hypernuclei: $A \gtrsim 200$), as shown in Table III. The experimental bands include values of the non–mesonic widths which are compatible with the quoted
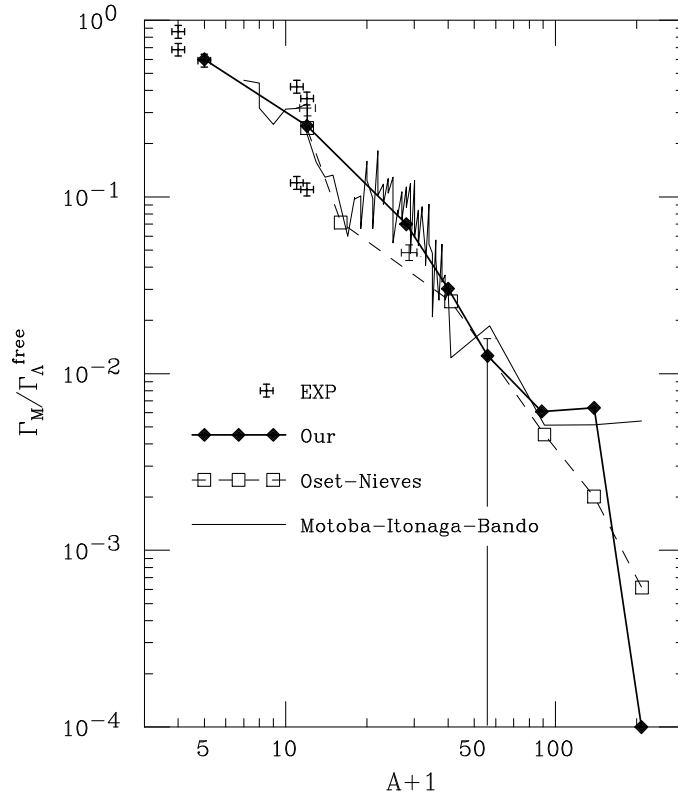
Fig. 8. – Mesonic width as a function of the nuclear mass number A. The results of Ref. [5, 27] (thick solid line) are compared with the calculations of Nieves–Oset [8] (dashed line) and Motoba–Itonaga–Bandō [9, 43] (solid line). Available experimental data [37, 38, 41] are also shown. See text for details on data (taken from Ref. [5]).

experiments. For medium and heavy hypernuclei the available experimental data actually refer to the *total* decay rate. However, the mesonic width for medium hypernuclei is at most 5% of the total width and rapidly decreases as A increases. Hence, one can safely approximate $\Gamma_{NM}^{\mathrm{exp}}$ with Γ_T^{exp} for medium and heavy systems. In the third column of Table III we report the average Fermi momenta obtained with Eq. (44). According to the Table, in Ref. [28] the following average Fermi momenta have been employed: $k_F = 1.1$ fm^{-1} for medium–light, $k_F = 1.2$ fm^{-1} for medium and $k_F = 1.36$ fm^{-1} for heavy hypernuclei.

In addition to $\langle k_F \rangle$, other parameters enter into the microscopic calculation of hypernuclear decay widths, which are specifically related to the baryon–meson vertices and to the short range correlations. With the exception of the Landau parameters g' and g'_Λ, the values of these parameters have been kept fixed on the basis of the existing
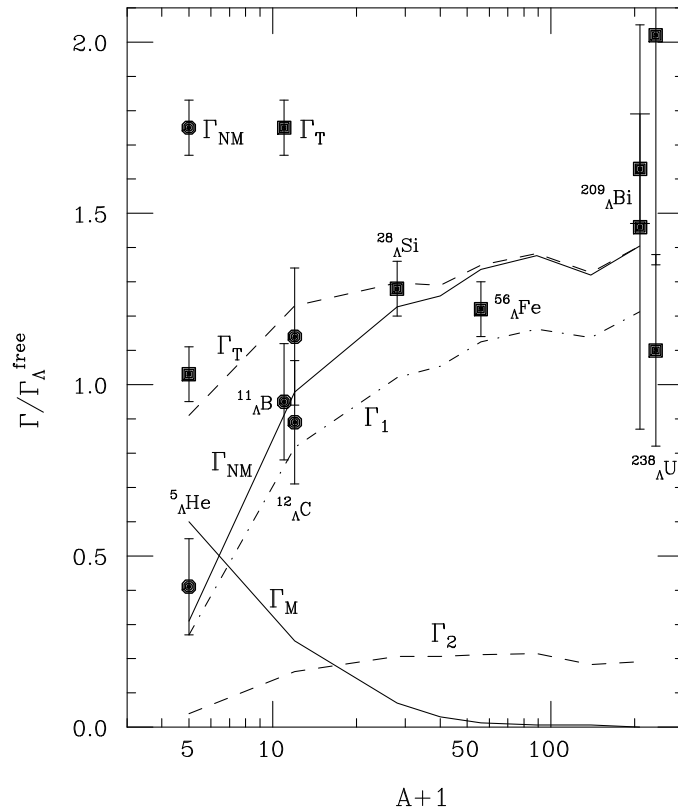
Fig. 9. – Partial Λ decay widths in finite nuclei as a function of the nuclear mass number A. Experimental data are from Refs. [37–39, 45, 46] (taken from Ref. [5]).

Table III. – *Average Fermi momenta for three representative mass regions. The experimental data are in units of the free Λ decay rate (taken from Ref. [28]).*

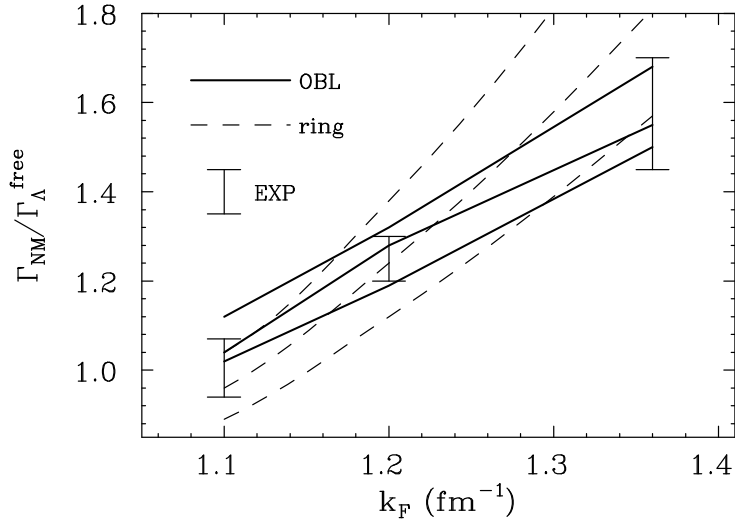|	Γ_{NM}^{exp}	$\langle k_F \rangle$ (fm^{-1})
Medium–Light: $^{11}_{\Lambda}$B - $^{12}_{\Lambda}$C	$0.94 \div 1.07$ [37, 38]	1.08
Medium : $^{28}_{\Lambda}$Si - $^{56}_{\Lambda}$Fe	$1.20 \div 1.30$ [39]	$\simeq 1.2$
Heavy: $^{209}_{\Lambda}$Bi - $^{238}_{\Lambda}$U	$1.45 \div 1.70$ [45, 46]	1.36

Fig. 10. – Dependence of the non–mesonic width on the Fermi momentum of nuclear matter. The solid curves refer to the one–boson–loop approximation (with $g' = 0.7, 0.8, 0.9$ from the top to the bottom), while the dashed lines refer to the ring approximation ($g' = 0.5, 0.6, 0.7$). The experimental data are also shown (taken from Ref. [28]).

phenomenology (for example in the analysis of quasi–elastic electron–nucleus scattering, spin–isospin nuclear response functions, etc). For the complete list of these quantities we refer the reader to Ref. [28].

Instead, the zero energy and momentum limits of the strong NN and ΛN correlations, g' and g'_Λ, are considered as *free parameters*. We remind the reader that the physical meaning of these Landau parameters is different in the present scheme (see Fig. 7) with respect to the customary phenomenology based on the ring approximation.

Fixing $g'_\Lambda = 0.4$, in ring approximation the experimental decay rates can be reproduced by using g' values which are compatible with the existing literature ($0.5 \leq g' \leq 0.7$). However, larger g' values ($0.7 \leq g' \leq 0.9$) appear to be more appropriate in the framework of the full OBL approximation. In addition, the OBL calculation allows for a good description (keeping the same g' value) of the rates in the whole range of k_F considered here.

In Fig. 10 we see the dependence of the non–mesonic widths on the Fermi momentum. The solid lines correspond to the OBL approximation, with $g' = 0.7, 0.8, 0.9$ from the top to the bottom, while the dashed lines refer to the ring approximation, with $g' = 0.5, 0.6, 0.7$, again from the top to the bottom. One can then conclude that for the OBL calculation the best choice for the Landau parameters is the following one: $g' = 0.8$, $g'_\Lambda = 0.4$. Accidentally, this parameterization turns out to be the same employed in the phenomenological evaluation of the *2p–2h* polarization propagator, although the

TABLE IV. – *Mesonic decay rate for $^{5}_{\Lambda}He$.*

Ref.	$\Gamma_M/\Gamma_\Lambda^{\text{free}}$	Model
Oset–Salcedo 1985 [24]	0.65	PPM
Oset–Salcedo–Usmani 1986 [49]	0.54	PPM
Itonaga–Motoba–Bandō 1988 [43]	$0.331 \div 0.472$	WFM
Motoba *et al.* 1991 [47]	0.608	WFM + Quark Model
Motoba 1992 [48]	0.61	WFM
Straub *et al.* 1993 [42]	0.670	WFM + Quark Model
Kumagai–Fuse *et al.* 1995 [50]	0.60	WFM
Exp BNL 1991 [37]	$0.59^{+0.44}_{-0.31}$	
Exp KEK 2004 [51]	0.541 ± 0.019	

role of strong short range correlations is different in the two approaches.

4˙3. *Other evaluations*. – In this subsection we briefly discuss how other calculations —performed within the Polarization Propagator Model (PPM) and the Wave Function Model (WFM) previously illustrated— compare with existing data.

In Table IV results for the mesonic decay width for $^{5}_{\Lambda}$He are reported. All the theoretical evaluations agree with the BNL datum but discrepancies appear if one compares them with the more accurate KEK observation. A repulsive core in the Λ–α mean potential (used in all but the calculation of Ref. [24]) is favoured. Moreover, it comes out naturally in the quark model descriptions of Refs. [42, 47]. The results of Refs. [43, 48] refer to the use of different pion–nucleus optical potentials. On this point, we note that the more recent datum is able to discriminate between different pion–nucleus optical potentials. Thanks to such precise determinations of Γ_{M}, novel information on this potential will be possibly extracted in the next future. The experimental and theoretical values of the ratio $\Gamma_{\pi^-}/\Gamma_{\pi^0}$, not shown in the table, do not deviate much from the $\Delta I = 1/2$ value ($= 2$) for free decays. We expect this result, since $^{5}_{\Lambda}$He has a closed shell core with $N = Z$.

The theoretical results for the mesonic rate for $^{12}_{\Lambda}$C, reported in Table V, are fairly compatible with data. The most notable exception is the calculation of Ref. [52], supplying a decay rate which strongly underestimates the KEK data. Also in this case, accurate measurements such as the one of Ref. [51] would provide important information on the pion–nucleon optical potential. The estimates obtained with the WFM of Refs. [8, 9, 43] are consistent with the experimental ratio $(\Gamma_{\pi^0}/\Gamma_{\pi^-})^{\text{Exp}} \simeq 1 \div 2 > (\Gamma_{\pi^0}/\Gamma_{\pi^-})^{\text{free}} = 1/2$, which reflects the particular nuclear shell structure of $^{12}_{\Lambda}$C.

Table VI refers to the non–mesonic rate for $^{5}_{\Lambda}$He, $^{12}_{\Lambda}$C and nuclear matter. The different $\Lambda N \to nN$ potentials used in the calculations reflect in a broad spectrum of predictions. In particular, Dalitz [55] (and more recently Jun *et al.* [56]) used a phe-

TABLE V. – *Mesonic decay rate for $^{12}_{\Lambda}C$.*

Ref.	$\Gamma_M/\Gamma_\Lambda^{\text{free}}$	Model
Oset–Salcedo 1985 [24]	0.41	PPM
Itonaga–Motoba–Bandō 1988 [43]	$0.233 \div 0.303$	WFM
Ericson–Bandō 1990 [53]	0.229	WFM
Nieves–Oset 1993 [8]	0.245	WFM
Itonaga–Motoba 1994 [9]	0.228	WFM
Ramos *et al.* 1995 [26]	0.31	PPM
Zhou–Piekarewicz 1999 [52]	0.112	Relativistic PPM
Albertus *et al.* 2003 [54]	0.25	WFM
Exp BNL 1991 [37]	0.11 ± 0.27	
Exp KEK 1995 [38]	0.36 ± 0.13	
Exp KEK 2004 [41]	0.313 ± 0.070	
Exp KEK 2004 [51]	0.288 ± 0.017	

nomenological model in which the OPE model at large distances is supplemented by a 4–baryon point interaction (4BPI) for the short range $\Lambda N \to nN$ interactions. Ref. [20] used a hybrid model in which the long range interactions are treated in terms of the OPE, while the short range interactions are described by a 6–quark cluster model which includes both $\Delta I = 1/2$ and $\Delta I = 3/2$ components. The PPM of Ref. [24] overestimate the data, although the decay rate is reduced when a more realistic Λ–wave function (less superimposed with the nuclear core) is used [27, 28, 49], and particularly if different short range correlations are considered [27, 28] (see results discussed in subsections **4**˙1 and **4**˙2). Antisymmetrization of the final nucleons, as in Ref. [18], would also moderately decrease the non–mesonic rate. Sasaki *et al.* [21] treated the non–mesonic decay within a direct quark (DQ) model combined with a OME potential containing pion and kaon exchange. In their model the NN and ΛN repulsion at short distance originates from quark exchange between baryons (induced by the quark anti–symmetrization) and gluon exchange between quarks. The intervals shown for the OME calculation of Ref. [17] correspond to the use of different Nijmegen models for the hadronic coupling constants. Itonaga *et al.* [16] considered the correlated two–pion–exchange.

Large part of the predictions of Table VI agree with the available data. The non–mesonic width in $^{12}_{\Lambda}$C seems to be reduced by a factor of about 2 with respect to the nuclear matter value. From inspection of data on heavy hypernuclei one concludes that realistic values of the Λ decay rate in nuclear matter lie in the range $1.5 \div 2$. From both experiment and theory, it also follow that $\Gamma_{\text{NM}}(^{12}_{\Lambda}\text{C}) \simeq 2\,\Gamma_{\text{NM}}(^{5}_{\Lambda}\text{He})$.

Table VI. – *Non–mesonic decay rate for $^5_\Lambda He$, $^{12}_\Lambda C$ and nuclear matter in units of the free Λ decay width.*

Ref. and Model	$^5_\Lambda$He	$^{12}_\Lambda$C	Nuclear Matter
Dalitz 1973 [55]	0.5		2
(WFM: OPE + 4BPI)			
Cheung *et al.* 1983 [20]		1.28	3
(WFM: hybrid)			
Oset–Salcedo 1985 [24]	1.15	1.5	2.2
(PPM: Correlated OPE)			
Oset–Salcedo–Usmani 1986 [49]	0.54		
(PPM: Correlated OPE)			
Sasaki *et al.* 2000 [21]	0.519		2.456
(WFM: $\pi + K+$ DQ)			
Jun *et al.* 2001 [56]	0.426	1.174	
(WFM: OPE + 4BPI)			
Jido *et al.* 2001 [18]		0.769	
(PPM: $\pi + K + 2\pi + \omega$)			
Parreño–Ramos 2001 [17]	$0.317 \div 0.425$	$0.554 \div 0.726$	
(WFM: $\pi + \rho + K + K^* + \omega + \eta$)			
Itonaga *et al.* 2002 [16]	0.422	1.060	
(WFM: $\pi + 2\pi/\rho + 2\pi/\sigma + \omega$)			
Exp BNL 1991 [37]	0.41 ± 0.14	1.14 ± 0.20	
Exp CERN 1993 [45]			$\bar{p}$+Bi: $1.46^{+1.83}_{-0.52}$
			$\bar{p}$+U: $2.02^{+1.74}_{-0.63}$
Exp KEK 1995 [38]		0.89 ± 0.18	
Exp KEK 1995 [57]	0.50 ± 0.07		
Exp COSY 1998 [46]			p+Bi: $1.63^{+0.19}_{-0.14}$
Exp KEK 2000 [39, 40]		0.83 ± 0.11	$^{56}_\Lambda$Fe: 1.22 ± 0.08
Exp COSY 2001 [58]			p+Au: $2.02^{+0.56}_{-0.35}$
Exp COSY 2001 [59]			p+U: $1.91^{+0.28}_{-0.22}$
Exp KEK 2004 [51]	0.406 ± 0.020	0.953 ± 0.032	

5. – The ratio Γ_n/Γ_p

Up to very recent times, the main challenge of hypernuclear weak decay studies has been to provide a theoretical explanation of the large experimental values for the ratio Γ_n/Γ_p between the neutron– and the proton–induced decay widths. Until recently, the large uncertainties involved in the extraction of the ratio from data did not allow to

reach any definitive conclusion. The data were quite limited and not precise due to the difficulty of detecting the products of the non–mesonic decays, especially the neutrons. Moreover, up to now it has not been possible to distinguish between nucleons produced by the one–body induced and the (non–negligible) two–body induced decay mechanism. However, due to recent theoretical [16–18, 21, 60] and experimental [61–63] progress, we are now towards a solution of the Γ_n/Γ_p puzzle. In this section we review these important developments.

The one–pion–exchange approximation with the $\Delta I = 1/2$ rule provides small ratios:

$$(45) \qquad\qquad \left[\frac{\Gamma_n}{\Gamma_p}\right]^{\text{OPE}} \simeq 0.05 \div 0.20,$$

for all the considered systems. This is due to the $\Delta I = 1/2$ rule, which fixes the vertex ratio $V_{\Lambda\pi^-p}/V_{\Lambda\pi^0n} = -\sqrt{2}$ (both in S– and P–wave interactions), and to the particular form of the OPE potential, which has a strong tensor component requiring isospin 0 np pairs in the antisymmetric final state. In p–shell and heavier hypernuclei the relative ΛN $L = 1$ state is found to give only a small contribution to tensor transitions for the neutron–induced decay, so it cannot improve the OPE ratio. The contribution of the ΛN $L = 1$ relative state to Γ_{NM} seems to be of about $5 \div 15\%$ in p–shell hypernuclei [17]. For these systems we expect the dominance of the S–wave interaction in the initial state, due to the small ΛN relative momentum. By using a simple argument about the isospin structure of the transition $\Lambda N \to nN$ in OPE, it is possible to estimate that for pure $\Delta I = 3/2$ transitions ($V_{\Lambda\pi^-p}/V_{\Lambda\pi^0n} = 1/\sqrt{2}$) the OPE ratio can increase up to about 0.5. However, the OPE model with $\Delta I = 1/2$ couplings has been able to reproduce the one–body stimulated non–mesonic rates $\Gamma_1 = \Gamma_n + \Gamma_p$ for light and medium hypernuclei [16–18, 21, 27, 28].

Other interaction mechanisms beyond the OPE might then be responsible for the overestimation of Γ_p and the underestimation of Γ_n. Many attempts have been made up to now in order to solve the Γ_n/Γ_p puzzle. We recall here the inclusion in the $\Lambda N \to nN$ transition potential of mesons heavier than the pion [14–18], the inclusion of interaction terms that explicitly violate the $\Delta I = 1/2$ rule [19] and the description of the short range baryon–baryon interaction in terms of quark degrees of freedom [20, 21], which automatically introduces $\Delta I = 3/2$ contributions. It is important to note that a few calculations with $\Lambda N \to nN$ transition potentials including heavy–meson–exchange and/or direct quark contributions [16–18, 21] have improved the situation, without providing, nevertheless, a satisfactory explanation of the origin of the puzzle. The tensor component of K–exchange has opposite sign with respect to the one for π–exchange, resulting in a reduction of Γ_p. The parity violating $\Lambda N(^3S_1) \to nN(^3P_1)$ transition, which contributes to both the n– and p–induced processes, is considerably enhanced by K–exchange and direct quark mechanism and tends to increase Γ_n/Γ_p.

In table VII we summarize the calculations that predicted ratios considerably enhanced with respect to the OPE values. Experimental data are given for comparison. Almost all calculations reproduce the observed non–mesonic widths $\Gamma_n + \Gamma_p$, as one can

Table VII. – Γ_n/Γ_p ratio.

Ref. and Model	$^5_\Lambda$He	$^{12}_\Lambda$C
Sasaki et al. 2000 [21] $\pi + K +$ DQ	0.701	
Jido et al. 2001 [18] $\pi + K + 2\pi + \omega$		0.53
Parreño–Ramos 2001 [17] $\pi + \rho + K + K^* + \omega + \eta$	$0.343 \div 0.457$	$0.288 \div 0.341$
Itonaga et al. 2002 [16] $\pi + 2\pi/\rho + 2\pi/\sigma + \omega$	0.386	0.368
BNL 1991 [37]	0.93 ± 0.55	$1.33^{+1.12}_{-0.81}$
KEK 1995 [38]		$1.87^{+0.67}_{-1.16}$
KEK 1995 [57]	1.97 ± 0.67	
KEK 2004 [41]		0.87 ± 0.23
KEK 2004 (coincidence) [61] (with Garbarino et al. [60, 64] analysis)	0.40 ± 0.11	0.38 ± 0.14

see in Table VIII [we remind the reader that the experimental data should also include (at least a part) of the two–nucleon induced decay rate]. Although no calculation is able to explain the old data on Γ_n/Γ_p, some predictions are in agreement with the recent determinations [60, 64] from KEK nucleon coincidence data [61]. We discuss in detail these analyses in **5**˙2.2.

5˙1. *Two–body induced decay and nucleon final state interactions*. – The analysis of the ratio Γ_n/Γ_p is influenced by the two–nucleon induced process $\Lambda NN \to nNN$, whose experimental identification is rather difficult and it is a challenge for the future. By assuming that the meson produced in the weak vertex is mainly absorbed by an isoscalar np correlated pair (quasi–deuteron approximation), the three–body process turns out to be $\Lambda np \to nnp$, so that a considerable fraction of the measured neutrons could come from this channel and not only from $\Lambda n \to nn$ and $\Lambda p \to np$. In this way it might be possible to explain the large experimental Γ_n/Γ_p ratios, which originally have been analyzed without taking into account the two–body stimulated process. Nevertheless, the situation is far from being clear and simple, both from the theoretical and experimental viewpoints. The new non–mesonic mode was introduced in Ref. [44] and its calculation was improved in Ref. [26], where the authors found that the inclusion of the new channel would bring to extract from the experiment even larger values for the Γ_n/Γ_p ratios, thus worsening the disagreement with the theoretical estimates. However, in the hypothesis that only two out of the three nucleons coming from $\Lambda np \to nnp$ are detected [65], the

TABLE VIII. – *Non–mesonic width $\Gamma_n + \Gamma_p$ (in units of $\Gamma_\Lambda^{\rm free}$)*.

Ref. and Model	$^5_\Lambda$He	$^{12}_\Lambda$C
Sasaki *et al.* 2000 [21] $\pi + K+$ DQ	0.519	
Jido *et al.* 2001 [18] $\pi + K + 2\pi + \omega$		0.769
Parreño–Ramos 2001 [17] $\pi + \rho + K + K^* + \omega + \eta$	$0.317 \div 0.425$	$0.554 \div 0.726$
Itonaga *et al.* 2002 [16] $\pi + 2\pi/\rho + 2\pi/\sigma + \omega$	0.422	1.060
BNL 1991 [37]	0.41 ± 0.14	1.14 ± 0.20
KEK 1995 [38]		0.89 ± 0.18
KEK 1995 [57]	0.50 ± 0.07	
KEK 2000 [40]		0.83 ± 0.11
KEK 2004 [51]	0.406 ± 0.020	0.953 ± 0.032

reanalysis of the experimental data would lead back to smaller ratios.

These observations show that Γ_n/Γ_p is sensitive to the detailed kinematics of the non–mesonic processes and to the experimental threshold for nucleon detection. In Ref. [66] the nucleon energy distributions have been calculated by using a Monte Carlo simulation to describe the nucleon rescattering inside the nucleus: the ratio Γ_n/Γ_p has been taken as a free parameter and extracted by comparing the simulated spectra with data. The momentum distributions of the primary nucleons were determined within the polarization propagator scheme. In their way out of the nucleus, the nucleons, due to the collisions with other nucleons, continuously change energy, direction, charge, and secondary nucleons are emitted as well. Then, the energy distribution of the observable nucleons, which also loose their energy by the interactions with the experimental set–up, is quite different from the one at the level of the primary nucleons. The nucleons from two–body stimulated decays appear mainly at low energies, while those from the one–nucleon stimulated process peak around 75 MeV only for light hypernuclei such as $^5_\Lambda$He.

Quite recently, at KEK–E307 [67], the proton spectra for $^{12}_\Lambda$C, $^{28}_\Lambda$Si and $^{56}_\Lambda$Fe were measured and compared with theoretical simulations of the intranuclear cascades after the weak processes, obtained with the MC code of Ref. [66]. Corrections for the detector geometry and the nucleon interactions inside the target and detector materials were necessary: they were implemented through a GEANT MC code. After fitting the KEK–E307 spectra using Γ_n/Γ_p as a free parameter, the following results were obtained [41]

by neglecting the two–nucleon induced decay channel:

(46)
$$\frac{\Gamma_n}{\Gamma_p}(^{12}_\Lambda\text{C}) = 0.87 \pm 0.23,$$

$$\frac{\Gamma_n}{\Gamma_p}(^{28}_\Lambda\text{Si}) = 0.79^{+0.28}_{-0.26},$$

$$\frac{\Gamma_n}{\Gamma_p}(^{56}_\Lambda\text{Fe}) = 1.13^{+0.29}_{-0.27}.$$

All the existing calculations underestimate the $^{12}_\Lambda$C result (see Table VII). The Γ_n/Γ_p ratios of Eq. (46) confirm the results of previous experiments: the neutron– and proton–induced decay rates appear to be of the same order of magnitude over a large hypernuclear mass number range. However, since the new experiments have significantly improved the quality of the data, small values of Γ_n/Γ_p (say smaller than 0.5 for $^{12}_\Lambda$C, as predicted by theory) seem to be excluded.

5˙2. *Towards a solution of the Γ_n/Γ_p puzzle*. – Fortunately, recent important developments have contributed to approach the solution of the Γ_n/Γ_p puzzle. This progress has been based on the following main ideas:

1) The proton spectra originating from neutron– and proton–induced processes (and, eventually, from two–nucleon stimulated decays) are added *incoherently* in the Monte Carlo intranuclear cascade code used to determine Γ_n/Γ_p from data. In this way a possible quantum–mechanical *interference* effect between the two channels is lost. Therefore, extracting Γ_n/Γ_p from data with the help of a classical intranuclear cascade calculation may not be a clean task. The consequences of this idea have been explored in Ref. [60].

2) In order to perform, as desirable, a direct measurement of Γ_n/Γ_p one needs to detect the outgoing *neutrons*. In principle, neutron spectra can be measured down to about 10 MeV kinetic energy since they are less affected than the proton ones by energy losses in the target and detector materials. Besides, the joint observation of proton and neutron spectra could help to disentangle the set–up material effects from the nucleon FSI occurring inside the residual nucleus. A recent experiment, KEK–E369, measured neutron spectra from $^{12}_\Lambda$C and $^{89}_\Lambda$Y non–mesonic decays [62]. With other experiments, KEK–E462 and KEK–E408 [63], proton and neutron spectra could be simultaneously measured for $^{5}_\Lambda$He and $^{12}_\Lambda$C. An analysis of these data has been done in Ref. [60] and is discussed in **5**˙2.1.

3) One could avoid the possible deficiencies of the *single* nucleon spectra measurements discussed in point 1) by employing nucleon–nucleon *coincidence* measurements, which should indeed permit a cleaner extraction of Γ_n/Γ_p. Coincidence observations are also expected to be less affected by FSI effects and to help in the direct observation of two–nucleon induced decay events. In the experiments KEK–E462 and KEK–E508 [61], nn and np angular and energy correlation measurements

have been performed for the decay of $^5_\Lambda$He and $^{12}_\Lambda$C. Other experiments, at BNL [68] and J–PARC [69], will determine Γ_n/Γ_p for s–shell hypernuclei, again by nn and np coincidence measurements. More data are expected in the near future from DaΦne [70].

5˙2.1. *Analyses of single nucleon spectra.* In Ref. [60] a OME model for the $\Lambda N \to nN$ transition in finite nuclei was incorporated in the intranuclear cascade code of Ref. [66] for the calculation of single and coincidence nucleon distributions from hypernuclear non–mesonic weak decay. The OME weak transition potential [17] contained the exchange of π, ρ, K, K^*, ω and η mesons. Strong couplings and strong FSI acting between the weak decay nucleons were taken into account by means of a nN wave function from the Lippmann–Schwinger equation obtained with NSC97 (versions "a" and "f") potentials [71]. The two–nucleon stimulated channel is also taken into account, using the polarization propagator method and treating the nuclear finite size effects by means of a local density approximation.

Single neutron and proton spectra have been calculated and compared with data for $^5_\Lambda$He and $^{12}_\Lambda$C. In Fig. 11 we show results of Ref. [60] for the kinetic energy neutron distribution from $^{12}_\Lambda$C based on two models [OPE and OMEf (using the NSC97f potential)], which predict quite different Γ_n/Γ_p ratios. The KEK–E369 spectrum [62] is well reproduced by the calculations. Unfortunately, the dependence of the neutron spectrum N_n on variations of Γ_n/Γ_p is very weak (the same is true also for the proton spectrum) and a precise extraction of the ratio from the KEK–E369 distribution is not possible. The little sensitivity of N_n and N_p to Γ_n/Γ_p is mainly due to the fact that these numbers are normalized to the same total non–mesonic decay rate (i.e., per non–mesonic weak decay). The non–normalized nucleon spectra, $S_n \equiv N_n\,\Gamma_{\rm NM}$ and $S_p \equiv N_p\,\Gamma_{\rm NM}$ [see Eq. (47)], have indeed a stronger dependence on Γ_n/Γ_p. As a consequence, in order to discriminate between different weak decay models, one should separately compare the complementary observable, $\Gamma_{\rm NM}$, with experiment. For $^{12}_\Lambda$C, the calculations of Ref. [60] supply $\Gamma_{\rm NM} \equiv \Gamma_n + \Gamma_p + \Gamma_2 = 0.91$ or 0.69 when model OMEa or OMEf is used, which agree quite well with the experimental determinations (see Table VIII).

Let us now introduce the number of nucleons of the type N ($N = n, p$) produced in n–induced ($N_N^{1{\rm Bn}}$), p–induced ($N_N^{1{\rm Bp}}$) and two–nucleon induced ($N_N^{2{\rm B}}$) decays. If we normalize these quantities per n–induced, p–induced, and two–nucleon induced decay, respectively, the *total* number of nucleons of the type N (normalized per non–mesonic weak decay) is given by:

$$
(47) \qquad N_N = \frac{N_N^{1{\rm Bn}}\,\Gamma_n + N_N^{1{\rm Bp}}\,\Gamma_p + N_N^{2{\rm B}}\,\Gamma_2}{\Gamma_n + \Gamma_p + \Gamma_2}
$$
$$
\equiv N_N^{\Lambda n \to nn} + N_N^{\Lambda p \to np} + N_N^{\Lambda np \to nnp},
$$

where $N_N^{\Lambda n \to nn}$, $N_N^{\Lambda p \to np}$ and $N_N^{\Lambda np \to nnp}$ have obvious meaning and are shown in Fig. 11 for the neutron spectrum from $^{12}_\Lambda$C. All these nucleon numbers can be considered either as being functions of the nucleon kinetic energy, $N_N(T_N)$, as it is in Fig. 11, or as
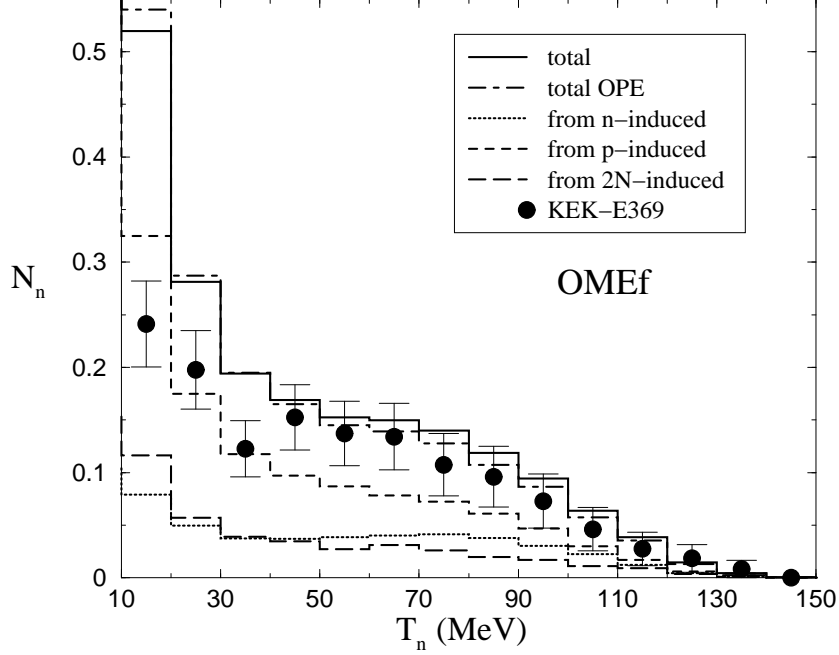
Fig. 11. – Single neutron kinetic energy spectra for the non–mesonic weak decay of $^{12}_{\Lambda}$C. The total spectrum N_n (normalized per non–mesonic weak decay) has been decomposed in its components $N_{np}^{\Lambda n \to nn}$, $N_{np}^{\Lambda p \to np}$ and $N_{np}^{\Lambda np \to nnp}$ according to Eq. (47) (taken from Ref. [60]).

the corresponding integrated quantities, $N_N = \int dT_N N_N(T_N)$. By construction, N_N^{1Bn}, N_N^{1Bp} and N_N^{2B} ($N_N^{\Lambda n \to nn}$, $N_N^{\Lambda p \to np}$ and $N_N^{\Lambda np \to nnp}$) *do not* depend (*do* depend) on the interaction model employed to describe the weak decay.

The problem of the small sensitivity of N_n and N_p to variations of Γ_n/Γ_p can be overcome if one concentrates on another single nucleon observable, the ratio N_n/N_p. The number of *weak decay* neutrons and protons produced per non–mesonic weak decay are given by $N_n^{\text{wd}} = (2\,\Gamma_n + \Gamma_p)/\Gamma_{\text{NM}}$ and $N_p^{\text{wd}} = \Gamma_p/\Gamma_{\text{NM}}$, respectively. Thus, the ratio Γ_n/Γ_p can be obtained as:

$$(48) \qquad \frac{\Gamma_n}{\Gamma_p} \equiv \frac{1}{2}\left(\frac{N_n^{\text{wd}}}{N_p^{\text{wd}}} - 1\right).$$

Due to two–body induced decays and (especially) nucleon FSI, one expects the inequality:

$$(49) \qquad \frac{\Gamma_n}{\Gamma_p} \neq \frac{1}{2}\left(\frac{N_n}{N_p} - 1\right) \equiv R_1\left[\Delta T_n, \Delta T_p\right]$$

to be valid in a situation, such as the experimental one, in which particular intervals of

TABLE IX. – *Predictions of Ref. [60] for the quantity R_1 of Eq. (49) for $^5_\Lambda$He corresponding to different nucleon kinetic energy thresholds T_N^{th} and to the OPE, OMEa and OMEf models.*

| | T_N^{th} (MeV) | | | |
	0	30	60	Γ_n/Γ_p
OPE	0.04	0.13	0.16	0.09
OMEa	0.15	0.32	0.39	0.34
OMEf	0.19	0.40	0.49	0.46
KEK–E462 [63]			0.59 ± 0.11	

variability of the neutron and proton kinetic energy, ΔT_n and ΔT_p, are employed in the determination of the *observable* numbers N_n and N_p.

The results of Ref. [60] clearly show a pronounced dependence of R_1 on ΔT_n and ΔT_p (see Table IX); N_n/N_p turns out to be much less sensitive to FSI effects and variations of the energy cuts than N_n and N_p separately. The OMEf prediction of Table IX corresponding to $T_N^{\mathrm{th}} = 60$ MeV is compatible with the very recent determination by KEK–E462 [63].

5˙2.2. *Analyses of coincidence spectra.* Due to the reduction of interferences and FSI effects, nucleon correlation analyses are expected to provide a cleaner determination of Γ_n/Γ_p than single nucleon observables [5]. Ref. [60] evaluated double–nucleon energy and angular correlations and analyzed the data obtained by the experiments KEK–E462 and KEK–E508 [61] for $^5_\Lambda$He and $^{12}_\Lambda$C.

In Fig. 12 we report the prediction of Ref. [60] for the kinetic energy correlation of np pairs emitted in the non–mesonic decay of $^{12}_\Lambda$C. To facilitate a comparison with experiments, whose kinetic energy threshold for proton (neutron) detection is typically of about 30 MeV (10 MeV), and to avoid a possible non–realistic behaviour of the intranuclear cascade simulation for low nucleon energies, the distributions correspond to T_n, $T_p \geq 30$ MeV. A narrow peak, mainly originated by the back–to–back kinematics ($\cos\theta_{np} < -0.8$) of the one–nucleon induced decay, is predicted around 155 MeV, i.e., close to the Q–value expected for the proton–induced three–body process $^{12}_\Lambda$C $\rightarrow ^{10}$B $+ n + p$. A broad peak, predominantly due to $\Lambda p \rightarrow np$ or $\Lambda n \rightarrow nn$ weak transitions followed by the emission of secondary (less energetic) nucleons, has been found around 110 MeV for $\cos\theta_{np} > -0.8$.

Figure 13 shows the opening angle correlations of nn, np and pp pairs from the non–mesonic weak decay of $^{12}_\Lambda$C and for a 30 MeV energy threshold. The peaking structure at $\cos\theta \simeq -1$ for the nn (np) distribution is a clear signal of the back–to–back kinematics of the neutron (proton) induced decay. For a discussion of the different effects of FSI in the energy and angular coincidence distributions for $^5_\Lambda$He and $^{12}_\Lambda$C see Ref. [60].
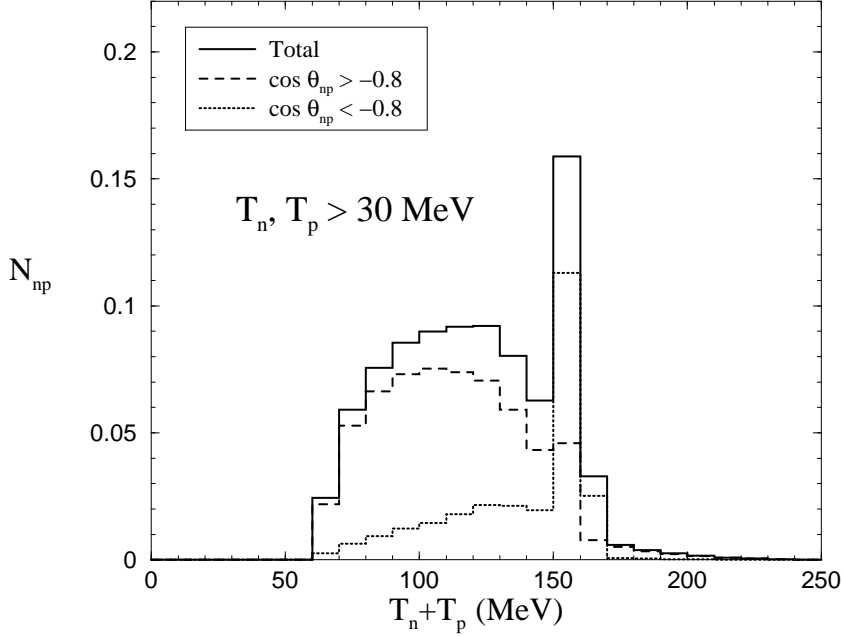
Fig. 12. – Kinetic energy correlations of np pairs emitted per non–mesonic decay of $^{12}_{\Lambda}C$ (taken from Ref. [60]).

The ratio Γ_n/Γ_p is defined as the ratio between the number of *weak decay nn* and *np* pairs, N_{nn}^{wd} and N_{np}^{wd}. However, due to two–body induced decays and (especially) nucleon FSI effects, one has:

$$(50) \qquad \frac{\Gamma_n}{\Gamma_p} \equiv \frac{N_{nn}^{\mathrm{wd}}}{N_{np}^{\mathrm{wd}}} \neq \frac{N_{nn}}{N_{np}} \equiv R_2 \left[\Delta\theta_{12}, \Delta T_n, \Delta T_p\right]$$

when the *observable* numbers N_{nn} and N_{np} are determined by employing particular intervals of variability of the pair opening angle, $\Delta\theta_{12}$, and the nucleon kinetic energies, ΔT_n and ΔT_p. The discussion of Ref. [60] proves that N_{nn}/N_{np} is much less sensitive to FSI effects and variations of the energy cuts and angular restrictions than N_{nn} and N_{np} separately.

The numbers of nucleon pairs N_{NN} discussed up to now and normalized per non–mesonic weak decay are related to the corresponding quantities for the one–nucleon (N_{NN}^{1B}) and two–nucleon (N_{NN}^{2B}) induced processes [the former (latter) being normalized per one–body (two–body) stimulated non–mesonic weak decay] via the following equation:

$$(51) \qquad N_{NN} = \frac{N_{NN}^{\mathrm{1B}}\,\Gamma_1 + N_{NN}^{\mathrm{2B}}\,\Gamma_2}{\Gamma_1 + \Gamma_2} \equiv N_{NN}^{\Lambda n \to nn} + N_{NN}^{\Lambda p \to np} + N_{NN}^{\Lambda np \to nnp},$$
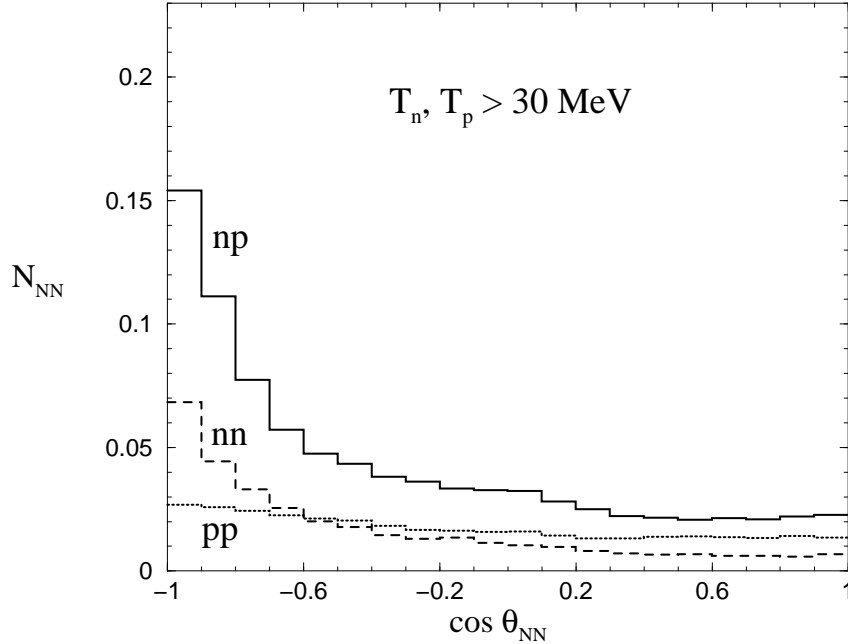
Fig. 13. – Opening angle correlations of *nn*, *np* and *pp* pairs emitted per non–mesonic decay of $^{12}_{\Lambda}$C (taken from Ref. [60]).

where:

$$(52) \qquad\qquad N^{1B}_{NN} = \frac{N^{1Bn}_{NN}\,\Gamma_n + N^{1Bp}_{NN}\,\Gamma_p}{\Gamma_1},$$

and the remaining N's have obvious meaning. Therefore, the quantities N^{1Bn}_{NN}, N^{1Bp}_{NN} and N^{2B}_{NN} ($N^{\Lambda n\rightarrow nn}_{NN}$, $N^{\Lambda p\rightarrow np}_{NN}$ and $N^{\Lambda np\rightarrow nnp}_{NN}$) *do not* depend (*do* depend) on the interaction model employed to describe the weak decay.

In Table X the ratio N_{nn}/N_{np} predicted by the OPE, OMEa and OMEf models of Refs. [60, 64] for $^{5}_{\Lambda}$He and $^{12}_{\Lambda}$C is given for a nucleon energy threshold of 30 MeV and for the back–to–back kinematics (cos $\theta_{NN} \leq -0.8$). The predictions of the different weak decay models for Γ_n/Γ_p are also quoted. The results of the OMEa and OMEf models are in agreement with the preliminary KEK–E462 and KEK–E508 data [61]: this comparison provides an indication for a ratio $\Gamma_n/\Gamma_p \simeq 0.3$ in both hypernuclei.

A weak–decay–model independent analysis of KEK coincidence data has been performed in Ref. [60]. The six weak–interaction–model independent quantities N^{1Bn}_{nn}, N^{1Bp}_{nn},

TABLE X. – *Predictions of Refs. [60, 64] for the ratio N_{nn}/N_{np} for $^{5}_{\Lambda}He$ and $^{12}_{\Lambda}C$. They correspond to an energy thresholds T_N^{th} of 30 MeV and to the back–to–back kinematics ($\cos\theta_{NN} \leq -0.8$). The (preliminary) data are from KEK–E462 and KEK–E508 [61].*

	$^{5}_{\Lambda}$He		$^{12}_{\Lambda}$C	
	N_{nn}/N_{np}	Γ_n/Γ_p	N_{nn}/N_{np}	Γ_n/Γ_p
OPE	0.25	0.09	0.24	0.08
OMEa	0.51	0.34	0.39	0.29
OMEf	0.61	0.46	0.43	0.34
EXP	0.45 ± 0.11		0.40 ± 0.09	

$N_{nn}^{2\text{B}}$, $N_{np}^{1\text{Bn}}$, $N_{np}^{1\text{Bp}}$ and $N_{np}^{2\text{B}}$ of Eqs. (51) and (52) are used to evaluate Γ_n/Γ_p as:

$$(53) \qquad \frac{\Gamma_n}{\Gamma_p} = \frac{N_{nn}^{1\text{Bp}} + N_{nn}^{2\text{B}}\dfrac{\Gamma_2}{\Gamma_1} - \left(N_{np}^{1\text{Bp}} + N_{np}^{2\text{B}}\dfrac{\Gamma_2}{\Gamma_1}\right)\dfrac{N_{nn}}{N_{np}}}{\left(N_{np}^{1\text{Bn}} + N_{np}^{2\text{B}}\dfrac{\Gamma_2}{\Gamma_1}\right)\dfrac{N_{nn}}{N_{np}} - N_{nn}^{1\text{Bn}} - N_{nn}^{2\text{B}}\dfrac{\Gamma_2}{\Gamma_1}}$$

[which can be easily obtained from Eqs. (51) and (52)], using appropriate values for Γ_2/Γ_1 and data for N_{nn}/N_{np}. For the KEK values of Table X the following ratios have been determined:

$$(54) \qquad \frac{\Gamma_n}{\Gamma_p}\left(^{5}_{\Lambda}\text{He}\right) = 0.40 \pm 0.11 \ \text{if}\ \Gamma_2 = 0 \ , \ \frac{\Gamma_n}{\Gamma_p}\left(^{5}_{\Lambda}\text{He}\right) = 0.27 \pm 0.11 \ \text{if}\ \frac{\Gamma_2}{\Gamma_1} = 0.2,$$

$$(55) \qquad \frac{\Gamma_n}{\Gamma_p}\left(^{12}_{\Lambda}\text{C}\right) = 0.38 \pm 0.14 \ \text{if}\ \Gamma_2 = 0 \ , \ \frac{\Gamma_n}{\Gamma_p}\left(^{12}_{\Lambda}\text{C}\right) = 0.29 \pm 0.14 \ \text{if}\ \frac{\Gamma_2}{\Gamma_1} = 0.25,$$

where the non–vanishing values adopted for Γ_2/Γ_1 are predictions obtained in Ref. [27] within the polarization propagator method in local density approximation. The Γ_n/Γ_p values of Eqs. (54) and (55) are in agreement with the pure theoretical predictions of Refs. [16–18] but are substantially smaller than those obtained experimentally from *single* nucleon spectra analyses (see Table VII). Actually, all the previous experimental analyses of single nucleon spectra, supplemented in some cases by intranuclear cascade calculations, derived Γ_n/Γ_p values in disagreement with all existing theoretical predictions. The fact that the calculations of Refs. [60, 64] reproduce coincidence data for values of Γ_n/Γ_p as small as $0.3 \div 0.4$ could signal the existence of non–negligible interference effects between the n– and p–induced channels in those old single nucleon data.

In our opinion, the achievements discussed in this subsection clearly exhibit the interest of analyses of correlation observables and represent an important progress towards

the solution of the Γ_n/Γ_p puzzle. Forthcoming coincidence data from KEK, BNL [68], J–PARC [69] and FINUDA [70] could be directly compared with the results discussed here and in Refs. [60, 64]. This will permit to achieve better determinations of Γ_n/Γ_p and to establish the first constraints on Γ_2/Γ_1.

6. – Hypernuclei of the s–shell and $\Delta I = 1/2$ rule

The analysis of the non–mesonic decays for s–shell hypernuclei offers an important and complementary tool for the solution of the Γ_n/Γ_p puzzle. In addition, it is very suitable for testing the validity of the related $\Delta I = 1/2$ rule.

For s–shell hypernuclei the ΛN pair is necessarily in the $L = 0$ relative state, thus the only possible $\Lambda N \to nN$ transitions are the following ones (we use the spectroscopic notation $^{2S+1}L_J$):

$$
\begin{aligned}
^1S_0 &\to {}^1S_0 \quad (I_f = 1) \\
&\to {}^3P_0 \quad (I_f = 1) \\
^3S_1 &\to {}^3S_1 \quad (I_f = 0) \\
&\to {}^1P_1 \quad (I_f = 0) \\
&\to {}^3P_1 \quad (I_f = 1) \\
&\to {}^3D_1 \quad (I_f = 0).
\end{aligned}
\tag{56}
$$

The $\Lambda n \to nn$ process has final states with isospin $I_f = 1$ only, while for $\Lambda p \to np$ both $I_f = 1$ and $I_f = 0$ are allowed.

6˙1. *Phenomenological model of Block and Dalitz*. – In the following we discuss an analysis performed by the authors [72] in order to explore the validity of the $\Delta I = 1/2$ rule in the one–nucleon induced Λ–decay. This analysis is based on a phenomenological model due to Block and Dalitz [73], which we briefly outline now.

The interaction probability of a particle which crosses an infinite homogeneous system of thickness ds is, classically, $dP = ds/\lambda$, where $\lambda = 1/(\sigma\rho)$ is the mean free path of the projectile, σ is the relevant cross section and ρ is the density of the system. Then, if we refer to the process $\Lambda N \to nN$, the width $\Gamma_{\rm NM} = dP_{\Lambda N \to nN}/dt$ can be written as:

$$
\Gamma_{\rm NM} = v\sigma\rho,
$$

$v = ds/dt$ being the Λ velocity in the rest frame of the homogeneous system. For a finite nucleus of density $\rho(\vec{r})$, after introducing a local Fermi sea of nucleons one can write, within the semiclassical approximation:

$$
\Gamma_{\rm NM} = \langle v\sigma \rangle \int d\vec{r}\rho(\vec{r}) \mid \psi_\Lambda(\vec{r}) \mid^2,
$$

where $\psi_\Lambda(\vec{r})$ is the Λ wave function in the hypernucleus and $\langle \rangle$ denotes an average over spin and isospin states. In the above equation the nuclear density is normalized to the

mass number $A = N + Z$, hence the integral gives the average nucleon density ρ_A at the position of the Λ hyperon. In this scheme, the non–mesonic width $\Gamma_{\mathrm{NM}} = \Gamma_n + \Gamma_p$ of the hypernucleus $^{A+1}_{\Lambda}Z$ turns out to be:

$$\Gamma_{\mathrm{NM}}(^{A+1}_{\Lambda}Z) = \frac{N\overline{R}_n(^{A+1}_{\Lambda}Z) + Z\overline{R}_p(^{A+1}_{\Lambda}Z)}{A}\rho_A,$$

where $\overline{R}_n$ ($\overline{R}_p$) denotes the spin–averaged rate for the neutron–induced (proton–induced) process appropriate for the considered hypernucleus.

Furthermore, by introducing the rates R_{NJ} for the spin–singlet (R_{n0}, R_{p0}) and spin–triplet (R_{n1}, R_{p1}) elementary $\Lambda N \to nN$ interactions, the non–mesonic decay widths of s–shell hypernuclei are [73]:

(57)
$$\Gamma_{\mathrm{NM}}(^{3}_{\Lambda}\mathrm{H}) = (3R_{n0} + R_{n1} + 3R_{p0} + R_{p1})\frac{\rho_2}{8},$$

$$\Gamma_{\mathrm{NM}}(^{4}_{\Lambda}\mathrm{H}) = (R_{n0} + 3R_{n1} + 2R_{p0})\frac{\rho_3}{6},$$

$$\Gamma_{\mathrm{NM}}(^{4}_{\Lambda}\mathrm{He}) = (2R_{n0} + R_{p0} + 3R_{p1})\frac{\rho_3}{6},$$

$$\Gamma_{\mathrm{NM}}(^{5}_{\Lambda}\mathrm{He}) = (R_{n0} + 3R_{n1} + R_{p0} + 3R_{p1})\frac{\rho_4}{8}.$$

These relations take into account that the total hypernuclear angular momentum is 0 for $^{4}_{\Lambda}\mathrm{H}$ and $^{4}_{\Lambda}\mathrm{He}$ and 1/2 for $^{3}_{\Lambda}\mathrm{H}$ and $^{5}_{\Lambda}\mathrm{He}$. In terms of the rates associated to the partial–wave transitions (56), the R_{NJ}'s of Eqs. (57) read:

$$R_{n0} = R_n(^1S_0) + R_n(^3P_0),$$
$$R_{p0} = R_p(^1S_0) + R_p(^3P_0),$$
$$R_{n1} = R_n(^3P_1),$$
$$R_{p1} = R_p(^3S_1) + R_p(^1P_1) + R_p(^3P_1) + R_p(^3D_1),$$

the quantum numbers of the nN final state being reported in brackets.

If one assumes that the $\Lambda N \to nN$ weak interaction occurs with a change $\Delta I = 1/2$ of the isospin, the following relations (simply derived by angular momentum coupling coefficients) hold among the rates for transitions to $I_f = 1$ final states:

(58) $$R_n(^1S_0) = 2R_p(^1S_0), \quad R_n(^3P_0) = 2R_p(^3P_0), \quad R_n(^3P_1) = 2R_p(^3P_1).$$

Hence:

(59)
$$\frac{R_{n1}}{R_{p1}} \leq \frac{R_{n0}}{R_{p0}} = 2.$$

TABLE XI. – *Experimental data for the non–mesonic weak decay of s–shell hypernuclei.*

	$\Gamma_n/\Gamma_\Lambda^{\text{free}}$	$\Gamma_p/\Gamma_\Lambda^{\text{free}}$	$\Gamma_{\text{NM}}/\Gamma_\Lambda^{\text{free}}$	Γ_n/Γ_p	Ref.
$^4_\Lambda\text{H}$			0.22 ± 0.09		reference value
			0.17 ± 0.11		KEK [11]
			0.29 ± 0.14		[73]
$^4_\Lambda\text{He}$	0.04 ± 0.02	0.16 ± 0.02	0.20 ± 0.03	0.25 ± 0.13	BNL [74]
$^5_\Lambda\text{He}$	0.20 ± 0.11	0.21 ± 0.07	0.41 ± 0.14	0.93 ± 0.55	BNL [37]

For pure $\Delta I = 3/2$ transitions, the factors 2 in Eqs. (58) are replaced by $1/2$. Then, by further introducing the ratio:

$$r = \frac{\langle I_f = 1 || A_{1/2} || I_i = 1/2 \rangle}{\langle I_f = 1 || A_{3/2} || I_i = 1/2 \rangle}$$

between the $\Delta I = 1/2$ and $\Delta I = 3/2$ $\Lambda N \to nN$ transition amplitudes for isospin 1 final states (r being real, as required by time reversal invariance), for a general $\Delta I = 1/2$–$3/2$ isospin mixture one gets:

$$(60) \qquad \frac{R_{n1}}{R_{p1}} = \frac{4r^2 - 4r + 1}{2r^2 + 4r + 2 + 6\lambda^2} \leq \frac{R_{n0}}{R_{p0}} = \frac{4r^2 - 4r + 1}{2r^2 + 4r + 2},$$

where:

$$(61) \qquad \lambda = \frac{\langle I_f = 0 || A_{1/2} || I_i = 1/2 \rangle}{\langle I_f = 1 || A_{3/2} || I_i = 1/2 \rangle}.$$

The partial rates of Eq. (60) supply Γ_n/Γ_p for s–shell hypernuclei through Eqs. (57).

By using Eqs. (57) and (60) together with available data it is possible to determine the spin–isospin structure of the $\Lambda N \to nN$ interaction without resorting to a detailed knowledge of the interaction mechanism.

6˙2. *Experimental data and $\Delta I = 1/2$ rule*. – In Ref. [72] a phenomenological analysis of the data summarized in Table XI is employed to study the possible violation of the $\Delta I = 1/2$ rule in the process $\Lambda N \to nN$.

Unfortunately, no data are available on the non–mesonic decay of hypertriton ($^3_\Lambda\text{H}$) and on Γ_n/Γ_p for $^4_\Lambda\text{H}$. Indeed, we shall see in the following that future measurements of Γ_n/Γ_p for $^4_\Lambda\text{H}$ at BNL [68] and J–PARC [69] will be of great importance for testing the $\Delta I = 1/2$ rule. The BNL data [37, 74] for $^4_\Lambda\text{He}$ and $^5_\Lambda\text{He}$ of Table XI together with the *reference value* for $^4_\Lambda\text{H}$ have been used in the analysis of Ref. [72]. This last number is the weighted average of two previous estimates [11, 73], which have not been obtained from direct measurements but rather by using theoretical constraints. One has then 5

independent data which allow to fix, from Eqs. (57), the 4 rates $R_{N,J}$ and ρ_3. Indeed, the average nucleon density at the Λ position for $^5_\Lambda$He, also entering Eqs. (57), has been estimated to be $\rho_4 = 0.045$ fm^{-3} by employing the Λ wave function of Ref. [42] (which was obtained through a quark model description of the ΛN interaction) and the gaussian density for ^{4}He that reproduces the experimental mean square radius of the nucleus. For $^4_\Lambda$H and $^4_\Lambda$He, instead, no realistic hyperon wave function is available and we can obtain the value $\rho_3 = 0.026$ fm^{-3} from the data of Table XI, by imposing that [see Eqs. (57)]:

$$\frac{\Gamma_p(^5_\Lambda\text{He})}{\Gamma_p(^4_\Lambda\text{He})} = \frac{3}{4}\frac{\rho_4}{\rho_3}.$$

The best choice to determine the rates $R_{N,J}$ by fitting measured values corresponds to use the relations for the observables:

$$\Gamma_{\text{NM}}(^4_\Lambda\text{H}), \quad \Gamma_{\text{NM}}(^4_\Lambda\text{He}), \quad \Gamma_{\text{NM}}(^5_\Lambda\text{He}), \quad \frac{\Gamma_n}{\Gamma_p}(^4_\Lambda\text{He}),$$

which have the smallest experimental uncertainties. After solving these equations we obtained the following partial rates (as usual, the decay widths of Eqs. (57) are considered in units of the free Λ decay width):

$$(62) \qquad\qquad R_{n0} = (4.7 \pm 2.1) \text{ fm}^3,$$

$$(63) \qquad\qquad R_{p0} = (7.9^{+16.5}_{-7.9}) \text{ fm}^3,$$

$$(64) \qquad\qquad R_{n1} = (10.3 \pm 8.6) \text{ fm}^3,$$

$$(65) \qquad\qquad R_{p1} = (9.8 \pm 5.5) \text{ fm}^3,$$

$$\overline{R}_n(^5_\Lambda\text{He}) \equiv \frac{1}{4}\left(R_{n0} + 3R_{n1}\right) = (8.9 \pm 6.5) \text{ fm}^3,$$

$$\overline{R}_p(^5_\Lambda\text{He}) \equiv \frac{1}{4}\left(R_{p0} + 3R_{p1}\right) = (9.3 \pm 5.8) \text{ fm}^3.$$

The errors have been obtained with the standard method, i.e., by treating the data as independent and uncorrelated.

For the ratios of Eq. (60) we have then:

$$(66) \qquad\qquad \frac{R_{n0}}{R_{p0}} = 0.6^{+1.3}_{-0.6},$$

$$(67) \qquad\qquad \frac{R_{n1}}{R_{p1}} = 1.0^{+1.1}_{-1.0}.$$

while the ratios of the spin–triplet to the spin–singlet interaction rates are:

$$\frac{R_{n1}}{R_{n0}} = 2.2 \pm 2.1,$$

$$\frac{R_{p1}}{R_{p0}} = 1.2^{+2.7}_{-1.2}.$$

The large uncertainties do not allow to draw definite conclusions about the possible violation of the $\Delta I = 1/2$ rule and the spin–dependence of the transition rates. Eqs. (66) and (67) are still compatible with Eq. (59), namely with the $\Delta I = 1/2$ rule, although the central value in Eq. (66) is more in agreement either with a pure $\Delta I = 3/2$ transition ($r \simeq 0$) or with $r \simeq 2$ [see Eq. (60)]. Actually, Eq. (66) is compatible with r in the range $-1/4 \div 40$, while the ratio λ of Eqs. (60) and (61) is completely undetermined.

By using the results of Eqs. (62)–(65) one predicts:

$$\frac{\Gamma_n}{\Gamma_p}(^3_\Lambda\text{H}) = 0.7^{+1.1}_{-0.7},$$

$$\frac{\Gamma_n}{\Gamma_p}(^4_\Lambda\text{H}) = 2.3^{+5.0}_{-2.3},$$

$$\frac{\Gamma_n}{\Gamma_p}(^5_\Lambda\text{He}) = 0.95 \pm 0.92,$$

and, by using $\rho_2 = 0.001$ fm^{-3} [73],

$$\Gamma_{\text{NM}}(^3_\Lambda\text{H}) = 0.007 \pm 0.006.$$

The ratio obtained for $^5_\Lambda$He is in agreement with the data of Table XI and with the recent determinations discussed in 5˙2.2. An accurate measurement of $\Gamma_{\text{NM}}(^3_\Lambda\text{H})$ and Γ_n/Γ_p for $^3_\Lambda$H and $^4_\Lambda$H would then provide a test of the weak decay model of Eqs. (57) if the rates of Eqs. (62)–(65) could be extracted with less uncertainty from data.

The compatibility of the data with the $\Delta I = 1/2$ rule can be discussed in a different way: by *assuming* this rule, we fix $R_{n0}/R_{p0} = 2$. Then, by using the observables:

$$\Gamma_{\text{NM}}(^4_\Lambda\text{He}), \quad \Gamma_{\text{NM}}(^5_\Lambda\text{He}), \quad \frac{\Gamma_n}{\Gamma_p}(^4_\Lambda\text{He}),$$

the extracted partial rates are (R_{n0}, R_{n1}, $\overline{R}_n$ and $\overline{R}_p$ are unchanged with respect to the above derivation):

$$R_{n0} = (4.7 \pm 2.1)\,\text{fm}^3,$$
$$R_{p0} \equiv R_{n0}/2 = (2.3 \pm 1.0)\,\text{fm}^3,$$
$$R_{n1} = (10.3 \pm 8.6)\,\text{fm}^3,$$
$$R_{p1} = (11.7 \pm 2.4)\,\text{fm}^3.$$

These values are compatible with the ones in Eqs. (62)–(65). For pure $\Delta I = 1/2$ transitions the spin–triplet interactions seem to dominate over the spin–singlet ones:

$$\frac{R_{n1}}{R_{n0}} = 2.2 \pm 2.1,$$

$$\frac{R_{p1}}{R_{p0}} = 5.0 \pm 2.4.$$

Moreover, since:

$$\frac{R_{n1}}{R_{p1}} = 0.9 \pm 0.8,$$

from Eq. (60) one obtains the following estimate for the ratio between the $\Delta I = 1/2$ amplitudes:

$$\left| \frac{\langle I_f = 0 || A_{1/2} || I_i = 1/2 \rangle}{\langle I_f = 1 || A_{1/2} || I_i = 1/2 \rangle} \right| \simeq \frac{1}{3.7} \div 2.3.$$

The other independent observables which have not been utilized are then predicted to be:

$$\Gamma_{\text{NM}}(^4_\Lambda \text{H}) = 0.17 \pm 0.11,$$

(68)
$$\frac{\Gamma_n}{\Gamma_p}(^5_\Lambda \text{He}) = 0.95 \pm 0.72,$$

in agreement with the data of Table XI, with a χ^2 for one degree of freedom of 0.31 (corresponding to a $0.56\,\sigma$ deviation). This means that these data are consistent with the hypothesis of validity of the $\Delta I = 1/2$ rule at the level of 60%. In other words, the $\Delta I = 1/2$ rule is excluded at the 40% confidence level. On the contrary, if, according to the analysis of subsection **5**˙2.2, one compares with the datum $\Gamma_n/\Gamma_p = 0.40 \pm 0.11$ for $^5_\Lambda$He, the $\Delta I = 1/2$ rule turns out to be completely excluded by the central value of Eq (68).

The observables for which experimental data are not available at present are predicted to be:

$$\frac{\Gamma_n}{\Gamma_p}(^3_\Lambda \text{H}) = 1.3 \pm 0.6,$$

$$\frac{\Gamma_n}{\Gamma_p}(^4_\Lambda \text{H}) = 7.6 \pm 6.2,$$

and, for $\rho_2 = 0.001$ fm^{-3},

$$\Gamma_{\text{NM}}(^3_\Lambda \text{H}) = 0.005 \pm 0.003.$$

We note that the central value of Γ_n/Γ_p for $^4_\Lambda$H in the analysis which enforces the $\Delta I = 1/2$ rule is considerably larger than the central value obtained in the general analysis previously discussed. Thus, the future measurements [68, 69] of this quantity will represent an important test of the $\Delta I = 1/2$ rule.

7. – Non–mesonic decay of polarized Λ–hypernuclei: the asymmetry puzzle

Lambda hypernuclear states can be produced with a sizeable amount of polarization [75]. The development of angular distribution measurements of decay particles (photons, pions and protons) from polarized hypernuclei is of crucial importance in order to extract new information on hypernuclear production, structure and decay.

Despite the recent progress discussed in section **5**, the reaction mechanism for the non–mesonic weak decay does not seem to be fully understood. Indeed, a new intriguing problem, of more recent origin, is open: it concerns a strong disagreement between theory and experiment on the asymmetry of the angular emission of non–mesonic decay protons from polarized hypernuclei. This asymmetry is due to the interference between parity–violating and parity–conserving $\vec{\Lambda}p \rightarrow np$ transition amplitudes [76]. The non–mesonic rates Γ_n and Γ_p are dominated by parity–conserving amplitudes. The study of the asymmetric emission of protons from polarized hypernuclei, with its information on the spin–parity structure of the $\Lambda p \rightarrow np$ process, is thus supposed to provide new constraints on the dynamics of the non–mesonic decay.

Thanks to the large momentum transfer involved, the $n(\pi^+, K^+)\Lambda$ reaction has been used [77, 78], at $p_\pi = 1.05$ GeV and small K^+ laboratory scattering angles ($2° \lesssim \theta_K \lesssim 15°$), to produce hypernuclear states with a substantial amount of spin–polarization preferentially aligned along the axis normal to the reaction plane. The origin of hypernuclear polarization is twofold [75]. It is known that the distortions (absorptions) of the initial (π^+) and final (K^+) meson–waves produce a small polarization of the hypernuclear orbital angular momentum up to laboratory scattering angles $\theta_K \simeq 15°$ (at larger scattering angles, the orbital polarization increases with a negative sign). At small but non–zero angles, the main source of polarization is due to an appreciable spin–flip term in the elementary reaction $\pi^+ n \rightarrow \Lambda K^+$, which interferes with the spin–nonflip amplitude. In a typical experimental situation with $p_\pi = 1.05$ GeV and $\theta_K \simeq 15°$, the polarization of the hyperon spin in the free $\pi^+ n \rightarrow \Lambda K^+$ process is about 0.75.

7˙1. *Spin–polarization observables*. – The intensity of protons emitted in $\vec{\Lambda}p \rightarrow np$ decays along a direction forming an angle Θ with the polarization axis is given by (see Ref. [79] for more details):

$$(69) \qquad I(\Theta, J) = I_0(J) \left[1 + \mathcal{A}(\Theta, J) \right],$$

where

$$(70) \qquad I_0(J) = \frac{\sum_M \sigma(J, M)}{2J + 1}$$

is the (isotropic) intensity for an unpolarized hypernucleus. In Eq. (70):

$$\sigma(J, M) = \sum_F |\langle F|\mathcal{M}|I; J, M\rangle|^2$$

is the intensity of protons emitted along the quantization axis for a projection M of the hypernuclear total spin J. The proton asymmetry parameter, $\mathcal{A}$, can be written in the following form [79]:

$$(71) \qquad \mathcal{A}(\Theta, J) = P_y(J) \, A_y(J) \cos \Theta.$$

The quantity:

$$A_y(J) = \frac{3}{J+1} \frac{\sum_M M \, \sigma(J, M)}{\sum_M \sigma(J, M)},$$

which is a property of the hypernuclear non–mesonic decay only, is usually referred to as the hypernuclear asymmetry parameter. The hypernuclear polarization P_y depends both on the kinematics (p_π and θ_K) and dynamics of the production reaction.

In the shell model weak–coupling scheme, P_y is directly related to the polarization p_Λ of the Λ spin in the hypernucleus as follows:

$$(72) \qquad p_\Lambda(J) = \begin{cases} -\dfrac{J}{J+1} P_y(J) & \text{if } J = J_C - \tfrac{1}{2} \\ P_y(J) & \text{if } J = J_C + \tfrac{1}{2}, \end{cases}$$

J_C being the total spin of the nuclear core. It is useful to introduce an *intrinsic lambda asymmetry parameter* a_Λ, which is characteristic of the elementary process $\vec{\Lambda} p \to np$ and should be independent of the hypernucleus, such that:

$$(73) \qquad \mathcal{A}(\Theta, J) = p_\Lambda(J) \, a_\Lambda \cos \Theta.$$

From Eqs. (71) and (72) it follows then:

$$a_\Lambda = \begin{cases} -\dfrac{J+1}{J} A_y(J) & \text{if } J = J_C - \tfrac{1}{2} \\ A_y(J) & \text{if } J = J_C + \tfrac{1}{2}. \end{cases}$$

7`2. *Experiment versus theory.* – Nucleon FSI acting after the non–mesonic weak decay are expected to modify the weak decay intensity of Eq. (69). Experimentally one has access to a proton intensity $I^M(\Theta, J)$ which is generally assumed to have the same Θ–dependence as $I(\Theta, J)$:

$$(74) \qquad I^M(\Theta, J) = I_0^M(J) \left[1 + p_\Lambda(J) \, a_\Lambda^M(J) \cos \Theta \right].$$

The observable asymmetry, $a_\Lambda^M(J)$, which is expected to depend on the hypernucleus, is then determined as:

$$(75) \qquad a_\Lambda^M(J) = \frac{1}{p_\Lambda(J)} \frac{I^M(0°, J) - I^M(180°, J)}{I^M(0°, J) + I^M(180°, J)}.$$

TABLE XII. – *Theoretical and experimental determinations of the asymmetry parameters (a_Λ and a_Λ^M, respectively). The predictions for a_Λ have been obtained with different OME weak transition potentials and with the direct quark mechanism (DQ).*

Ref. and Model	$_{\Lambda}^{5}\vec{\mathrm{He}}$	$_{\Lambda}^{12}\vec{\mathrm{C}}$
Sasaki et al. [21]		
$\pi + K + \mathrm{DQ}$	-0.68	
Parreño et al. [17]		
$\pi + \rho + K + K^* + \omega + \eta$	-0.68	-0.73
Itonaga et al. [81]		
$\pi + K + 2\pi/\rho + 2\pi/\sigma + \omega$	-0.33	
Barbero et al. [82]		
$\pi + \rho + K + K^* + \omega + \eta$	-0.54	
KEK–E160 [77]		$-0.9 \pm 0.3\,^*$
KEK–E278 [78]	0.24 ± 0.22	
KEK–E462 (preliminary) [80]	0.07 ± 0.08	
KEK–E508 (preliminary) [80]		-0.44 ± 0.32

* This result correspond to the weighted average (discussed on pag. 95 of Ref. [5]) among different p–shell hypernuclear data.

Until now, four KEK experiments measured the proton asymmetric emission from polarized Λ–hypernuclei. The experiment KEK–E160 [77], which studied p–shell hypernuclei, suffered from large uncertainties: only poor statistics and energy resolution could be used; moreover, the values of the Λ polarization p_Λ needed to determine the asymmetry a_Λ^M, had to be evaluated theoretically. More recently, a_Λ^M was measured by KEK–E278 [78] from the decay of $_{\Lambda}^{5}\vec{\mathrm{He}}$. The values of p_Λ used to obtain a_Λ^M were determined by observing the asymmetry, $\mathcal{A}^{\pi^-} = p_\Lambda\, a_\Lambda^{\pi^-}$, in the emission of negative pions in the $_{\Lambda}^{5}\vec{\mathrm{He}}$ mesonic decay, after assuming $a_\Lambda^{\pi^-}$ to be equal to the value for the free $\Lambda \to \pi^- p$ decay, $\alpha_{\pi^-} = -0.642 \pm 0.013$. Unfortunately, the small branching ratio and expected asymmetry $\mathcal{A}^{\pi^-}$ for the mesonic decay of p–shell hypernuclei makes a similar measurement of p_Λ very difficult for these systems; even the recent and more accurate experiment KEK–E508 [80] had to resort to theoretical estimates for the Λ polarization in $_{\Lambda}^{12}\vec{\mathrm{C}}$ and $_{\Lambda}^{11}\vec{\mathrm{B}}$. In the other recent experiment KEK–E462 [80], a_Λ^M was measured again for $_{\Lambda}^{5}\vec{\mathrm{He}}$, but with improved statistics.

In Table XII we report the results for a_Λ^M obtained by the above mentioned experiments together with available theoretical estimates for a_Λ. While theory predicts a negative intrinsic Λ asymmetry, with a moderate dependence on the hypernucleus, the measurements seem to favor positive values for $a_\Lambda^M(_{\Lambda}^{5}\vec{\mathrm{He}})$ and negative values for $a_\Lambda^M(_{\Lambda}^{12}\vec{\mathrm{C}})$.

7'3. *Recent developments*. – Concerning the above comparison between theory and experiment, it is important to stress that, while one predicts $a_\Lambda(_{\Lambda}^{5}\vec{\mathrm{He}}) \simeq a_\Lambda(_{\Lambda}^{12}\vec{\mathrm{C}})$, there

TABLE XIII. – *Results of Ref. [64] for the proton intensities [Eqs. (69) and (74)] from the non–mesonic weak decay of $^5_\Lambda\vec{\text{He}}$ and $^{12}_\Lambda\vec{\text{C}}$.*

	$^5_\Lambda\vec{\text{He}}$ I_0^{M}	a_Λ^{M}	$^{12}_\Lambda\vec{\text{C}}$ I_0^{M}	a_Λ^{M}
Without FSI	$I_0 = 0.69$	$a_\Lambda = -0.68$	$I_0 = 0.75$	$a_\Lambda = -0.73$
FSI and $T_p^{\text{th}} = 0$	1.27	-0.30	2.78	-0.16
FSI and $T_p^{\text{th}} = 30$ MeV	0.77	-0.46	1.05	-0.37
FSI and $T_p^{\text{th}} = 50$ MeV	0.59	-0.52	0.65	-0.51
FSI and $T_p^{\text{th}} = 70$ MeV	0.39	-0.55	0.38	-0.65
KEK–E462 (preliminary) [80]		0.07 ± 0.08		
KEK–E508 (preliminary) [80]				-0.44 ± 0.32

is no known reason to expect this approximate equality to be valid for a_Λ^{M}. Indeed, the relationship between $I(\Theta, J)$ of Eq. (69) and $I^{\text{M}}(\Theta, J)$ of Eq. (74) can be strongly affected by FSI of the emitted protons: this fact prevents establishing a direct relation between a_Λ and a_Λ^{M} and to make a direct comparison among results for these quantities. In order to overcome this obstacle, an evaluation of the effects of the nucleon FSI on the non–mesonic weak decay of $^5_\Lambda\vec{\text{He}}$, $^{11}_\Lambda\vec{\text{B}}$ and $^{12}_\Lambda\vec{\text{C}}$ has been performed very recently [64]. We summarize here some results of this investigation, which is the first one evaluating a_Λ^{M}.

The simulated proton intensities turned out to be well fitted by Eq. (74), then one can actually evaluate a_Λ^{M} through Eq. (75). In Table XIII we show predictions of the OMEf model (a OME model built with the NSC97f potential) for the weak decay and observable proton intensities, $I(\Theta, J)$ and $I^{\text{M}}(\Theta, J)$, respectively. As a result of the nucleon rescattering in the nucleus, $|a_\Lambda| \gtrsim |a_\Lambda^{\text{M}}|$ for any value of the proton kinetic energy threshold: when $T_p^{\text{th}} = 0$, $a_\Lambda/a_\Lambda^{\text{M}} \simeq 2$ for $^5_\Lambda\vec{\text{He}}$ and $a_\Lambda/a_\Lambda^{\text{M}} \simeq 4$ for $^{12}_\Lambda\vec{\text{C}}$; $|a_\Lambda^{\text{M}}|$ increases with T_p^{th} and $a_\Lambda/a_\Lambda^{\text{M}} \simeq 1$ for $T_p^{\text{th}} = 70$ MeV in both cases. Asymmetries a_Λ^{M} rather independent of the hypernucleus are obtained for $T_p^{\text{th}} = 30$, 50 and 70 MeV. The KEK data quoted in the table refer to a T_p^{th} varying between 30 and 50 MeV: the corresponding predictions of Ref. [64] agree with the $^{12}_\Lambda\vec{\text{C}}$ datum but are inconsistent with the observation for $^5_\Lambda\vec{\text{He}}$.

In conclusion, nucleon FSI turn out to be an important ingredient also when studying the non–mesonic weak decay of polarized hypernuclei, but they cannot explain the present asymmetry data. Further investigations are then required to clarify the issue. On the theoretical side there seems to be no reaction mechanism which may be responsible for positive or vanishing asymmetry values. On the experimental side the present anomalous discrepancy between different data needs to be resolved. Future experimental studies of the inverse reaction $\vec{p}n \to p\Lambda$ should also be encouraged, since they could help in disentangling the puzzling situation. Indeed, the weak production of the Λ–hyperon

could give a richer and cleaner (with respect to the non–mesonic hypernuclear decay) piece of information on the lambda–nucleon weak interaction and especially on the Λ polarization observables [83].

8. – Summary and perspectives

In these Lectures we have discussed several aspects of the weak decay of Λ–hypernuclei. Beyond the mesonic channel, which is observed also for a free Λ, the hypernuclear decay proceeds through non–mesonic processes, mainly induced by the interaction of the Λ with one nucleon or with a pair of correlated nucleons. This channel is the dominant one in medium–heavy hypernuclei, where the Pauli principle strongly suppresses the mesonic decay.

Various models have been proposed to describe the mesonic and non–mesonic decay rates as well as the asymmetry parameters in the decay of the Λ–hyperon in nuclei. The results obtained within these models have been thoroughly discussed. The mesonic rates have been reproduced quite well by calculations performed in different frameworks. Also the non–mesonic rates have been considered within a variety of phenomenological and microscopic models. In this context, particular interest has been devoted to the ratio Γ_n/Γ_p. Indeed, in spite of the fact that several calculations were able to reproduce, already at the OPE level, the total non–mesonic width, $\Gamma_{NM} = \Gamma_n + \Gamma_p(+\Gamma_2)$, the values therewith obtained for Γ_n/Γ_p revealed a strong disagreement with the experimental data. Although some of these calculations represented an improvement of the situation, further efforts were required in order to approach a solution the Γ_n/Γ_p puzzle. From the experimental side, recent experiments measured nucleon–nucleon coincidence observables with good statistics. Recent analyses of these data, complemented with the theoretical estimate of final state interactions, allowed the determination of Γ_n/Γ_p values in agreement with the theoretical expectations. Yet, good statistics coincidence measurements of nn and np emitted pairs are further required. These correlation measurements will also allow to establish the first constraints on the two–nucleon induced decay width, thus testing the various models which have been proposed for the evaluation of the different decay channels.

The analysis of the $\Delta I = 1/2$ rule in the non–mesonic decay of light hypernuclei appears to be feasible, also within a relatively simple phenomenological model: again, the measurements of a few delicate, missing decay rates, would help in understanding the role of this empirical selection rule.

As far as the decay of polarized hypernuclei is concerned, the situation is even more puzzling. While theory predicts negative values for both the intrinsic asymmetry a_Λ and the observable asymmetry a_Λ^{M}, with a moderate dependence on the hypernucleus, experiments seem to favour negative values for $a_\Lambda^{\mathrm{M}}(^{12}_{\Lambda}\vec{\mathrm{C}})$ but small, positive values for $a_\Lambda^{\mathrm{M}}(^{5}_{\Lambda}\vec{\mathrm{He}})$. Further investigations are then required to clarify the issue. Theoretically, there seems to be no reaction mechanism which may be responsible for positive or vanishing a_Λ^{M} values. Improved experiments, establishing with certainty the sign and magnitude of a_Λ^{M} for s– and p–shell hypernuclei, are strongly awaited.

We conclude this work by reminding the reader that hypernuclear physics is 52 years old, yet a lot of efforts remain to be done, both experimentally and theoretically, in order to fully understand the hyperon dynamics and decay inside the nuclear medium. The impressive progress experienced in the last few years is promising and we hope that it deserves a definite answer to the intriguing open questions which we have illustrated here.

* * *

REFERENCES

[1]   M. Danysz and J. Pniewski, *Philos. Mag.*, **44** (1953) 348.
[2]   A. Gal, These Proceedings.
[3]   T. Nagae, These Proceedings.
[4]   H. Outa, These Proceedings.
[5]   W. M. Alberico and G. Garbarino, *Phys. Rep.*, **369** (2002) 1.
[6]   F. J. Gillman and M. B. Wise, *Phys. Rev. D*, **20** (1979) 2392.
[7]   M. Cristoforetti, P. Faccioli, E. V. Shuryak and M. Traini, *Phys. Rev. D*, **70** (2004) 054016.
[8]   J. Nieves and E. Oset, *Phys. Rev. C*, **47** (1993) 1478.
[9]   T. Motoba and K. Itonaga, *Prog. Theor Phys. Suppl.*, **117** (1994) 477.
[10] Y. Akaishi and T. Yamazaki, *Prog. Part. Nucl. Phys.*, **39** (1997) 565.
[11] H. Outa *et al.*, *Nucl. Phys. A*, **639** (1998) 251c.
[12] J. Cohen, *Prog. Part. Nucl. Phys.*, **25** (1990) 139.
[13] E. Oset and A. Ramos, *Prog. Part. Nucl. Phys.*, **41** (1998) 191.
[14] J. F. Dubach, G. B. Feldman and B. R. Holstein, *Ann. Phys.*, **249** (1996) 146.
[15] A. Parreño, A. Ramos and C. Bennhold, *Phys. Rev. C*, **56** (1997) 339.
[16] K. Itonaga, T. Ueda and T. Motoba, *Phys. Rev. C*, **65** (2002) 034617.
[17] A. Parreño and A. Ramos, *Phys. Rev. C*, **65** (2002) 015204.
[18] D. Jido, E. Oset and J. E. Palomar, *Nucl. Phys. A*, **694** (2001) 525.
[19] A. Parreño, A. Ramos, C. Bennhold and K. Maltman, *Phys. Lett. B*, **435** (1998) 1.
[20] C.-Y. Cheung, D. P. Heddle and L. S. Kisslinger, *Phys. Rev. C*, **27** (1983) 335; D. P. Heddle and L. S. Kisslinger, *Phys. Rev. C*, **33** (1986) 608.
[21] K. Sasaki, T. Inoue and M. Oka, *Nucl. Phys. A*, **669** (2000) 331; **678** (2000) 455(E); **707** (2002) 477.
[22] E. Oset, H. Toki and W. Weise, *Phys. Rep.*, **83** (1982) 281.
[23] E. Oset, P. Fernández de Córdoba, J. Nieves, A. Ramos and L. L. Salcedo, *Prog. Theor. Phys. Suppl.*, **117** (1994) 461.
[24] E. Oset and L. L. Salcedo, *Nucl. Phys. A*, **443** (1985) 704.
[25] A. L. Fetter and J. D. Walecka, *Quantum Theory of Many Particle Systems* (McGraw–Hill, New York) 1971.
[26] A. Ramos, E. Oset and L. L. Salcedo, *Phys. Rev. C*, **50** (1994) 2314.
[27] W. M. Alberico, A De Pace, G. Garbarino and A. Ramos, *Phys. Rev. C*, **61** (2000) 044314.

[28] W. M. Alberico, A. De Pace, G. Garbarino and R. Cenni, *Nucl. Phys. A*, **668** (2000) 113.

[29] R. Seki and K. Masutani, *Phys. Rev. C*, **27** (1983) 2799.

[30] E. Friedman and A. Gal, *Nucl. Phys. A*, **724** (2003) 143

[31] C. Garcia-Recio, J. Nieves and E. Oset, *Nucl. Phys. A*, **547** (1992) 473.

[32] J. W. Negele, *Rev. Mod. Phys.*, **54** (1982) 813.

[33] W. M. Alberico, R. Cenni, A. Molinari and P. Saracco, *Ann. Phys.*, **174** (1987) 131.

[34] R. Cenni, F. Conte and P. Saracco, *Nucl. Phys. A*, **623** (1997) 391.

[35] C. B. Dover, A. Gal and D. J. Millener, *Phys. Rev. C*, **38** (1988) 2700.

[36] J. Vidaña, A. Polls, A. Ramos and M. Hjorth-Jensen, *Nucl. Phys. A*, **644** (1998) 201.

[37] J. J. Szymanski et al., *Phys. Rev. C*, **43** (1991) 849.

[38] H. Noumi et al., *Phys. Rev. C*, **52** (1995) 2936.

[39] H. C. Bhang et al., *Phys. Rev. Lett.*, **81** (1998) 4321; H. Park et al., *Phys. Rev. C*, **61** (2000) 054004.

[40] H. Outa et al., *Nucl. Phys. A*, **670** (2000) 281c.

[41] Y. Sato et al., **nucl–ex/0409007** (submitted to *Phys. Rev. C*).

[42] U. Straub, J. Nieves, A. Faessler and E. Oset, *Nucl. Phys. A*, **556** (1993) 531.

[43] K. Itonaga, T. Motoba and H. Bandō, *Z. Phys. A*, **330** (1988) 209; *Nucl. Phys. A*, **489** (1988) 683.

[44] W. M. Alberico, A. De Pace, M. Ericson and A. Molinari, *Phys. Lett. B*, **256** (1991) 134.

[45] T. A. Armstrong et al., *Phys. Rev. C*, **47** (1993) 1957.

[46] H. Ohm et al., *Phys. Rev. C*, **55** (1997) 3062; P. Kulessa et al., *Phys. Lett. B*, **427** (1998) 403.

[47] T. Motoba, H. Bandō, T. Fukuda and J. Žofka, *Nucl. Phys. A*, **534** (1991) 597.

[48] T. Motoba, *Nucl. Phys. A*, **547** (1992) 115c.

[49] E. Oset, L. L. Salcedo and Q. N. Usmani, *Nucl. Phys. A*, **450** (1986) 67c.

[50] I. Kumagai-Fuse, S. Okabe and Y. Akaishi, *Phys. Lett. B*, **345** (1995) 386.

[51] S. Okada et al., *VIII International Conference on Hypernuclear and Strange Particle Physics* (HYP2003), JLab, Newport News, Virginia, **nucl–ex/0402022** [*Nucl. Phys. A* (to be published)].

[52] L. Zhou and J. Piekarewicz, *Phys. Rev. C*, **60** (1999) 024306.

[53] M. Ericson and H. Bandō, *Phys. Lett. B*, **237** (1990) 169.

[54] C. Albertus, J. E. Amaro, and J. Nieves, *Phys. Rev. C*, **67** (2003) 034604.

[55] R. H. Dalitz, Proceedings of the *Summer Study Meeting on Nuclear and Hypernuclear Physics with Kaon Beams*, BNL Report No. 18335 (1973) p. 41.

[56] J.-H. Jun and H. C. Bhang, *Nuovo Cim.*, **112 A** (1999) 649; J.-H. Jun, *Phys. Rev. C*, **63** (2001) 044012.

[57] H. Noumi et al., Proceedings of the *IV International Symposium on Weak and Electromagnetic Interactions in Nuclei*, H. Ejiri, T. Kishimoto and T. Sato eds, World Scientific (1995) p. 550.

[58] B. Kamys et al., *Eur. Phys. J. A*, **11** (2001) 1.

[59] P. Kulessa et al., *Acta Phys. Polon. B*, **33** (2002) 603.

[60] G. Garbarino, A. Parreño and A. Ramos, *Phys. Rev. Lett.*, **91** (2003) 112501; *Phys. Rev. C*, **69** (2004) 054603.

[61] H. Outa, these proceedings and in *VIII International Conference on Hypernuclear and Strange Particle Physics* (HYP2003), JLab, Newport News, Virginia [*Nucl. Phys. A* (to be published)].

[62] J. H. Kim et al., *Phys. Rev. C*, **68** (2003) 065201.

[63] S. Okada et al., *Phys. Lett. B*, **597** (2004) 249.

[64] W. M. Alberico, G. Garbarino, A. Parreño and A. Ramos, *DAPHNE2004: Physics at meson factories*, Laboratori Nazionali di Frascati, Frascati, Italy, **nucl–th/0407046** [Frascati Physics Series (to be published)].

[65] A. Gal, in *Weak and electromagnetic interactions in nuclei*, H. Ejiri, T. Kishimoto and T. Sato eds, World Scientific (1995) p. 573.

[66] A. Ramos, M. J. Vicente–Vacas and E. Oset, *Phys. Rev. C*, **55** (1997) 735; **66** (2002) 039903E.

[67] O. Hashimoto et al., *Phys. Rev. Lett.*, **88** (2002) 042503.

[68] R. L. Gill, *Nucl. Phys. A*, **691** (2001) 180c.

[69] S. Ajimura, *Precise measurement of the non–mesonic weak decay of $A = 4, 5$ Λ–hypernuclei*, Letter of intent (LOI21) for experiments at J–PARC (2003).

[70] A. Zenoni, these proceedings; A. Feliciello, *Nucl. Phys. A*, **691** (2001) 170c; P. Gianotti, *Nucl. Phys. A*, **691** (2001) 483c.

[71] V. G. J. Stoks and Th. A. Rijken, *Phys. Rev. C*, **59** (1999) 3009.

[72] W. M. Alberico and G. Garbarino, *Phys. Lett. B*, **486** (2000) 362.

[73] M. M. Block and R. H. Dalitz, *Phys. Rev. Lett.*, **11** (1963) 96.

[74] V. J. Zeps, *Nucl. Phys. A*, **639** (1998) 261c.

[75] H. Bandō, T. Motoba M. Sotona and J. Žofka, *Phys. Rev. C*, **39** (1989) 587; H. Ejiri, T. Fukuda, T. Shibata, H. Bandō and K.-I. Kubo, *Phys. Rev. C*, **36** (1987) 1435.

[76] H. Bandō, T. Motoba and J. Žofka, *Int. J. Mod. Phys. A*, **5** (1990) 4021.

[77] S. Ajimura et al., *Phys. Lett. B*, **282** (1992) 293.

[78] S. Ajimura et al., *Phys. Rev. Lett.*, **84** (2000) 4052.

[79] A. Ramos, E. van Meijgaard, C. Bennhold and B. K. Jennings, *Nucl. Phys. A*, **544** (1992) 703.

[80] T. Maruta et al., *VIII International Conference on Hypernuclear and Strange Particle Physics* (HYP2003), JLAB, Newport News, Virginia, **nucl–ex/0402017** [*Nucl. Phys.* **A** (to be published)].

[81] K. Itonaga, T. Motoba and T. Ueda, in *Electrophoto–production of Strangeness on Nucleons and Nuclei* (Sendai03), K. Maeda, H. Tamura, S. N. Nakamura and O. Hashimoto eds, World Scientific (2004) p. 397.

[82] C. Barbero, C. De Conti, A. P. Galeão and F. Krmpotić, *Nucl. Phys. A*, **726** (2003) 267.

[83] H. Nabetani, T. Ogaito, T. Sato and T. Kishimoto, *Phys. Rev. C*, **60** (1999) 017001.